DNAJB12 and Hsp70 triage arrested intermediates of N1303K-CFTR for endoplasmic reticulum-associated autophagy

Lihua He†, Andrew S. Kennedy†, Scott Houck†, Andrei Aleksandrov, Nancy L. Quinney, Alexandra Cyr-Scully, Deborah M. Cholon, Martina Gentzsch, Scott H. Randell, Hong Yu Ren, and Douglas M. Cyr*

Department of Cell Biology and Physiology and the Cystic Fibrosis/Pulmonary Research and Treatment Center, University of North Carolina at Chapel Hill, Chapel Hill, NC 27599

ABSTRACT **The transmembrane Hsp40 DNAJB12 and cytosolic Hsp70 cooperate on the endoplasmic reticulum's (ER) cytoplasmic face to facilitate the triage of nascent polytopic membrane proteins for folding versus degradation. N1303K is a common mutation that causes misfolding of the ion channel CFTR, but unlike F508del-CFTR, biogenic and functional defects in N1303K-CFTR are resistant to correction by folding modulators. N1303K is reported to arrest CFTR folding at a late stage after partial assembly of its N-terminal domains. N1303K-CFTR intermediates are clients of JB12-Hsp70 complexes, maintained in a detergent-soluble state, and have a relatively long 3-h half-life. ER-associated degradation (ERAD)-resistant pools of N1303K-CFTR are concentrated in ER tubules that associate with autophagy initiation sites containing WIPI1, FIP200, and LC3. Destabilization of N1303K-CFTR or depletion of JB12 prevents entry of N1303K-CFTR into the membranes of ER-connected phagophores and traffic to autolysosomes. In contrast, the stabilization of intermediates with the modulator VX-809 promotes the association of N1303K-CFTR with autophagy initiation machinery. N1303K-CFTR is excluded from the ER-exit sites, and its passage from the ER to autolysosomes does not require ER-phagy receptors. DNAJB12 operates in biosynthetically active ER microdomains to triage membrane protein intermediates in a conformation-specific manner for secretion versus degradation via ERAD or selective-ER-associated autophagy.**

Monitoring Editor
James Olzmann
University of California, Berkeley

Received: Nov 3, 2020
Revised: Jan 19, 2021
Accepted: Jan 26, 2021

INTRODUCTION

Protein triage machines containing Hsp70 sort misfolded proteins between pathways for folding, degradation, and sequestration to suppress the accumulation of toxic species that kill cells (Klaips *et al.*, 2018). Inherited and spontaneous missense mutations cause misfolding of ion channels, P-Type ATPases, and G protein-coupled receptors, which underlie cystic fibrosis (CF), autoimmune disease, retinitis pigmentosa, hypercholesterolemia, and hypogonadism (Houck and Cyr, 2012). CF has been linked to over 1700 different mutations in the CFTR gene, with global misfolding and premature degradation of F508del-CFTR being the most common cause (Veit *et al.*, 2016). Folding modulators help overcome folding defects in F508del-NBD1 and, when used in combination with ion channel potentiators, restore CFTR function to therapeutic levels (Donaldson *et al.*, 2018; Keating *et al.*, 2018; Clancy *et al.*, 2019). However, it is not clear how changes in the conformation of a membrane protein elicited by a folding modulator would impact its recognition by molecular chaperones and sorting within the endoplasmic reticulum (ER) membrane system for secretion versus retention and degradation.

Assembly of polytopic membrane proteins is complicated because they expose surfaces that require the coordinated action of

This article was published online ahead of print in MBoC in Press (http://www.molbiolcell.org/cgi/doi/10.1091/mbc.E20-11-0688) on February 3, 2021.

†These authors contributed equally.

*Address correspondence to Douglas M. Cyr (DMCYR@med.unc.edu).

Abbreviations used: BSA, bovine serum albumin; CF, cystic fibrosis; CHX, cycloheximide; CL, cytoplasmic loop; CQ, chloroquine; Cys, cysteine; DTT, dithiothreitol; ER, endoplasmic reticulum; ERAD, ER-associated degradation; KBR, Krebs Bicarbonate Ringer; MSD, membrane-spanning domain; MTS, methanethiosulfonate; NBD, nucleotide-binding domain; PBS, phosphate-buffered saline; P_o, open probability.

cytosolic chaperones for folding, such as DNAJA1/Hsp70 (Meacham *et al.*, 1999), the ER transmembrane chaperone DNAJB12 (JB12) (Li *et al.*, 2017), an ER-luminal BIP, and calnexin (Daniels *et al.*, 2003; Houck and Cyr, 2012; Behnke *et al.*, 2016). These same chaperones also facilitate the selection of globally misfolded membrane protein intermediates for ER-associated degradation (ERAD) via the proteasome through interactions with quality control E3 ubiquitin-ligases (Meacham *et al.*, 2001; Cyr *et al.*, 2002; Younger *et al.*, 2006; Grove *et al.*, 2011). How Hsp70 and Hsp40 triage nonnative proteins between life and death are not entirely clear, but there are two significant determinants. The first is the folding kinetics for intermediates that are bound and released by Hsp70, with fast folding and limited rebinding to Hsp70 sparing nascent proteins from unnecessary degradation (Qian *et al.*, 2006). The second is the cellular set point for the expression of Hsp70 cochaperones that facilitate folding versus degradation (Meacham *et al.*, 2001; Buchberger, 2014).

It is generally assumed that globally misfolded proteins are recognized by the Hsp40-Hsp70 system, ubiquitinated by chaperone-dependent E3 ubiquitin ligases, and then threaded into the narrow cavity of the proteasome for degradation (Cyr *et al.*, 2002; Klaips *et al.*, 2018). In contrast, aggregated assemblies of misfolded proteins bury surfaces that are recognized by Hsp70 and cannot be translocated into the proteolytic chamber of the proteasomes, so they are degraded by endoproteases localized within autolysosomes (Pohl and Dikic, 2019; Wilkinson, 2019). However, intermediates of membrane proteins can accumulate in conformations containing tertiary structures (Gautier *et al.*, 2020). Intermediates with stable subdomains can be difficult to unfold and retrotranslocate into the cytosol and are therefore resistant to ERAD. Still, they are bound by molecular chaperones that suppress their aggregation and protect against ER-stress-induced apoptosis (Buchberger, 2014; Houck *et al.*, 2014). ERAD-resistant intermediates of a misfolded G-protein coupled receptor are stabilized by JB12-Hsp70 and degraded by an ER-associated autophagy pathway that is proposed to involve a functional interplay between JB12-Hsp70 with ER-associated autophagy initiation factors (Houck *et al.*, 2014). However, the mechanisms that govern the conformation-specific retention and triage of membrane proteins within biosynthetically active regions of the ER-tubular network are not clear.

CFTR is a 1480 amino acid anion channel containing two membrane-spanning domains (MSD1 and MSD2), two nucleotide-binding domains (NBD1 and NBD2), and a disordered regulatory R-domain. CFTR folding and misfolding is the topic of intense study, which has identified disease-causing mutations that cause arrested intermediates to accumulate in globally misfolded and aggregated states (Doonan *et al.*, 2019). The F508del mutation is located in NBD1, so F508del-NBD1 is unstable and fails to correctly assemble with NBD2 and the cytoplasmic loops (CL) that lie in between CFTR's 12 transmembrane spans. Folding modulators such as VX-809 partially restore F508del-CFTR folding by stabilizing MSD1 and F508del-NBD1, making more efficient the downstream assembly reactions involving contact formation of F508del-NBD1 with CLs (Ren *et al.*, 2013; Singh *et al.*, 2020). In contrast, N1303K, a common CF causing missense mutation located in NBD2 (Cutting, 2017), arrests CFTR folding at a late stage. Unfortunately, arrested intermediates of N1303K-CFTR exhibit resistance to repair by folding modulators (Veit *et al.*, 2016). CFTR assembly involves both cotranslational folding and posttranslational assembly of its NBDs, which occurs through the interaction of NBD1 and NBD2 with each other and different CLs (Cyr, 2005). NBD2 folding limits completion of CFTR assembly (Zhang *et al.*, 1998), so N1303K is likely to disrupt this process. But, how molecular chaperones triage and protect the ER from the accumulation of aggregated forms of late-stage intermediates whose posttranslation assembly arrests after folding initiation is a mystery.

To understand how ER protein quality control (ERQC) machinery triages globally misfolded versus arrested intermediates of membrane proteins, we conducted a detailed study of the biology and triage of N1303K-CFTR. These studies lead to the identification of the folding defect in N1303K-CFTR that causes it to stably associate with JB12-Hsp70 and be cleared from the ER membrane system by an ER-associated autophagy mechanism that is not dependent on ER-phagy receptors (Wilkinson, 2019). ER-associated-autophagy is distinct from ER-phagy because ER tubules containing N1303K-CFTR become clients of autophagy initiation machinery that is painted onto adjacent tubules that convert N1303K-CFTR containing tubules into phagophores containing LC3. Autophagosomes enriched in N1303K-CFTR and LC3 then bud from the ER and fuse with lysosomes that are docked to the WIPI1 rings on which they were formed. These results provide new insights into mechanisms by which Hsp70 and JB12 triage ERAD-resistant clients for degradation by ER-associated autophagy.

RESULTS

Impact of folding modulators and Cl-channel potentiators on N1303K-CFTR function

To initiate the evaluation of the functional and folding defects caused by N1303K, we measured the response of endogenous N1303K-CFTR expressed in native airway cells obtained from CF patients to folding modulators (Figure 1). Class I folding modulators stabilize MSD1 and NBD1 of CFTR to suppress the folding defects caused by F508del allosterically. Class II modulators appear to act synergistically with class I modulators to restore assembly of F508del-NBD1 with CL4 in MSD2 of CFTR. (Rosser *et al.*, 2008; Grove *et al.*, 2009; Ren *et al.*, 2013; Veit *et al.*, 2020). Modulators act on arrested intermediates of F508del-CFTR but do not rescue all CFTR mutants (Van Goor *et al.*, 2014). Therefore, insights into the nature of arrested N1303K-CFTR intermediates were obtained by evaluating their response to modulators.

Primary airway cells with the heterozygous N1303K/W1282X genotype were grown on semipermeable-supports at an air–liquid interface to permit the formation of a polarized and sealed cell monolayer. The response of the N1303K-CFTR function to modulators was evaluated in Ussing chambers (Fulcher *et al.*, 2005). CFTR is a cAMP-activated ion channel, so cells were treated with forskolin to stimulate transepithelial short-circuit currents, and N1303K-CFTR function was monitored in the absence or presence of indicated modulators (VX-809, class I, and C3, C4, Class II) (Gentzsch *et al.*, 2016; Singh *et al.*, 2020). W1282X-CFTR mRNA is truncated and subject to nonsense mediated decay, so W1282X CFTR does not accumulate in native airway cells (Oren *et al.*, 2017). N1303K-CFTR channel function is therefore evaluated in the absence of W1282X-CFTR in primary N1303K/W1282X cells. Results presented with primary N1303K/W1282X cells do not include a comparison to results with WT native airway cells. This is because CFTR activity in primary cells varies over a broad range due to differences in individual donors' lung biology and is in the range of 10 to 50 $\mu A/CM^2$ (Yu *et al.*, 2012; Veit *et al.*, 2020). Therefore, in primary cells, the change in forskolin-stimulated currents in the absence or presence of a modulator is utilized to evaluate drug efficacy on mutant CFTR. Forskolin-stimulated N1303K-CFTR chloride channel activity in polarized cell monolayers was not detected above the basal current (Figure 1A, black trace) and incubation of the cells with VX-809 for 48 h does not significantly increase forskolin-stimulated responses (Figure 1A

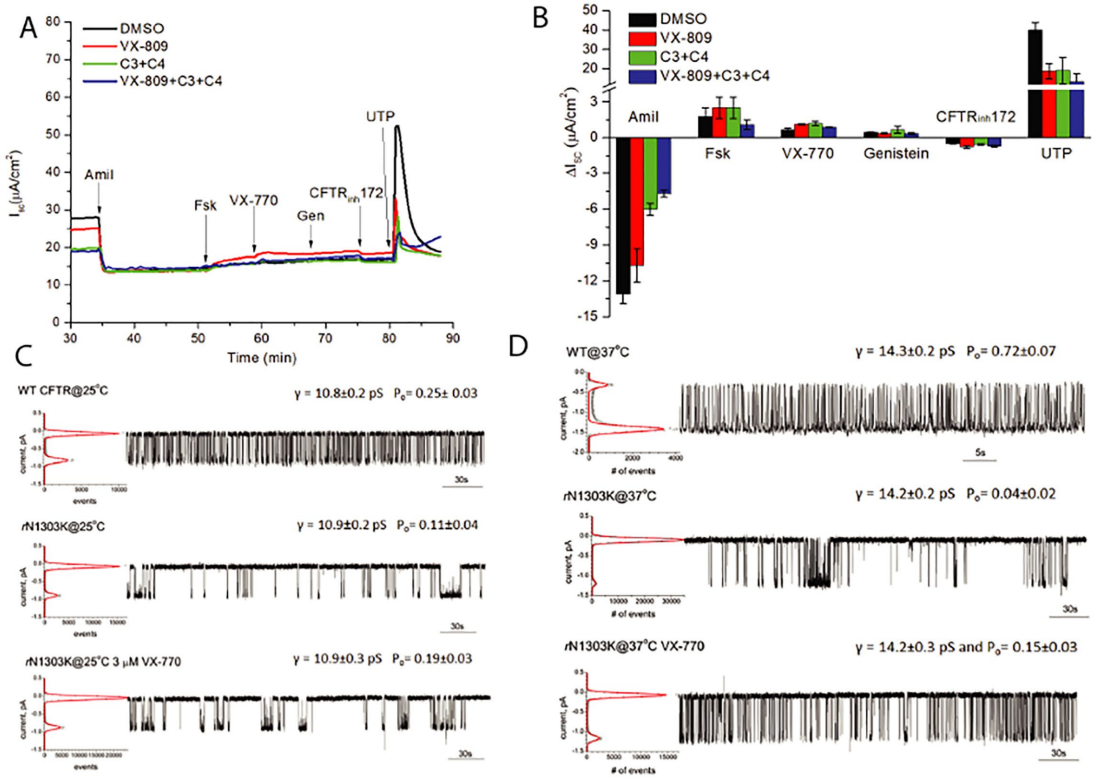

E

	25 °C		30 °C		37 °C	
	P_o	γ (pS)	P_o	γ (pS)	P_o	γ (pS)
WT-CFTR	0.25± 0.03	10.8±0.2	0.60± 0.05	12.3±0.2	0.72±0.07	14.3±0.2
rN1303K	0.11±0.04	10.9±0.2	0.07±0.03	12.2±0.2	0.04±0.02	14.2±0.2
rN1303K+ VX-770	0.19±0.03	10.9±0.3	0.23±0.04	12.3±0.2	0.15±0.03	14.2±0.3

FIGURE 1: Function of N1303K-CFTR is partially restored by cell culture at low temperature but is insensitive to folding modulators. (A) The effect of small molecule folding modulators and channel potentiators on CFTR activity in polarized native human bronchial epithelial (HBE) was measured in Ussing chambers. Representative traces illustrate the response of CFTR expressed in HBE treated with indicated compounds and CFTR channel activators (B): Bar graphs represent the mean net response ($n = 4$ cultures per corrector treatment) to acutely added stimuli or inhibitors in Ussing chamber experiments. HBE from patients carrying N1303K/W1282X mutations were chronically treated for 48 h with 3 μM VX-809, or 5 μM C3+C4, or 0.1% DMSO, as indicated. See Supplemental Figure S1A for Western blot analysis of the effect of correctors on N1303K/W1282X CFTR expression in HBE. (C) Single channel function of the WT and rescued N1303K (rN1303K) CFTR in the lipid bilayer. The ion channels were transferred into the preformed lipid bilayer by spontaneous fusion of membrane vesicles prepared from BHK cells stably expressing WT or rescued N1303K-CFTR. BHK cells expressing N1303K-CFTR was rescued by growing at 27°C in the presence of 5 μM C3 and C4 for the last 24 h before harvesting and labeled as rN1303K on the figure. Single channels were recorded at 25°C (C) or 37°C (D) for WT CFTR (top panel), rescued N1303K-CFTR (middle panel), and rescued N1303K-CFTR in the presence of VX-770 (bottom panel). The all points histogram used to calculate single channel conductance (γ) and P_o is shown on the left of the upper line of each group. The 5-min single channel recording used to prepare all points histogram is shown on the right of the upper line. Seven independent experiments of total 58 min duration, five independent experiments of total 35 min duration, and four independent experiments of total 17 min duration were used to calculate γ and Po of WT CFTR, rN1303K, and rN1303K+VX-770, respectively, at 25°C (C). Five independent experiments of total 42 min, four independent experiments of total 28 min duration, and three independent experiments with total 12 min duration were used to calculate γ and Po of WT CFTR, rN1303K, and rN1303K+VX-770, respectively, at 37°C (D). The difference in conductance between rN1303K and WT CFTR is not significant while the difference in Po is significant ($p < 0.05$). (E) Table summarizing the γ and Po of WT and rN1303K-CFTR measured at 25, 30, and 37°C.

and B, red trace and bar graph), nor does a mixture of class I and Class II modulators (Figure 1A, green trace and blue trace, respectively). The acute addition of VX-770, a drug that opens the CFTR channel, caused no significant boost in measured currents. N1303K-CFTR function is, therefore, not detected in the absence or the presence of modulators in primary lung cells. However, modulators appear to impact the conformation of N1303K-CFTR in native airway cells because they modestly increase the steady-state levels of the ER-localized B-form that is detected by Western blot (Supplemental Figure S1A).

Low-temperature cell culture permits some CFTR mutants to fold, escape the ER, and traffic to the plasma membrane

(Denning *et al.*, 1992). N1303K-CFTR was therefore stably expressed in BHK cells, and CFTR-expressing BHK cells were grown at 27°C, instead of 37°C, in the absence or the presence of modulators, which permitted modulators to stimulate the accumulation of the C-form of N1303K-CFTR (Supplemental Figure S1B). Single-channel measurements identified N1303K-CFTR channels in detergent-soluble extracts made from the plasma membranes of low-temperature BHK cells (Figure 1C). N1303K-CFTR channels exhibited the same conductance but an open probability (P_o) of less than half of WT CFTR (Figure 1C, top and middle panels). When the activity of reconstituted N1303K-CFTR channels was measured in single-channel recordings at temperatures from 25 to 37°C, the P_o of WT CFTR increased to 0.72. It remained stable during the time course of measurements (Figure 1D, top trace). However, the P_o for N1303K-CFTR decreased (Figure 1D, middle trace), and channel activity was less stable than WT-CFTR at 37°C. See Supplemental Figure S1C for channel recordings measured at 30°C. A summary of the P_o and conductance measured at different temperatures is presented in Figure 1E. Notably, the P_o of N1303K-CFTR was stabilized by VX-770 at 25, 30, and 37°C. These results suggest that N1303K-CFTR can assemble into a CFTR-like ion channel when thermal energy is low, and the fate of N1303K-CFTR intermediates is manipulatable.

N1303K-CFTR intermediates accumulate in a detergent-soluble and biochemically stable state

To evaluate the challenge presented to the ERQC machinery by late-stage intermediates of membrane proteins that fail to complete folding, we characterized the behavior of N1303K-CFTR in ER membranes of cells cultured at 37°C (Meacham *et al.*, 1999, 2001; Younger *et al.*, 2006; Ren *et al.*, 2013; Gentzsch *et al.*, 2016). N1303K-CFTR intermediates accumulated in an incompletely glycosylated state in the ER that is termed band B, which has faster electrophoretic mobility than the folded form, represented by band C. Band C is glycosylated further during passage through the Golgi on route to the plasma membrane (Figure 2 and Supplemental Figure S2) (Meacham *et al.*, 1999, 2001; Dalal *et al.*, 2004; Cyr, 2005). At T = 0, the levels of the B-form of N1303K-CFTR were severalfold higher than the B-form of F508del-CFTR (Figure 2A and Supplemental Figure S3). These differences were accounted for by the observed longer half-life of N1303K-CFTR (3 h) versus F508del-CFTR (1 h) in cycloheximide (CHX) chase experiments (Figure 2A). A short 2-h pretreatment with VX-809 (3 μM) further increased the stability of N1303K-CFTR such that at the end of 3-h CHX-chase, around 80% of B-band remained. VX-809 treatment increased the accumulation of the folded C-form of ΔF508-CFTR but only increased the half-life of its B-form to 1.5 h. VX-809 increased C-band levels of CFTR but did not cause the B-form of WT to accumulate (Supplemental Figure S2). At 37°C, N1303K-CFTR folds to an intermediate conformation that is stabilized by VX-809, but completion of CFTR assembly is blocked by N1303K.

To study the intracellular behavior of N1303K-CFTR via microscopy, EGFP-N1303K-CFTR and EGFP-F508del-CFTR were employed (Figures 2–7). In controls, untagged and EGFP-tagged CFTR behaved similarly (see below), so triage of EGFP-N1303K-CFTR and EGFP-F508del reflects the behavior of untagged CFTR.

The mobility of the ER-localized B-form of N1303K-CFTR and F508del-CFTR within the ER-tubular network was evaluated in live cells by monitoring rates of fluorescence recovery after photobleaching (Figure 2B). We evaluated the mobility of WT, F508del, and N1303K, and the raw microscopy data from experiments with F508del and N1303K are presented in Figure 2B. Data obtained with WT and F508del were similar, so raw data from WT CFTR are not shown. N1303K-CFTR does not disrupt ER morphology and the diffusion coefficients for WT, F508del, and N1303K-CFTR were 0.060 ± 0.003, 0.053 ± 0.006, and 0.084 ± 0.009 $\mu M^2/s$, respectively. The mobility of N1303K is faster than that of WT and F508del-CFTR at the 95% confidence level (see Figure 2 legend), so its nonspecific aggregation is not likely to contribute to its retention in the ER membrane system.

The aggregation state of N1303K-CFTR was also compared with that of CFTR and F508del-CFTR in cellular fractionation assays (Figure 2C). The assay protocol requires solubilization of cells in a nondenaturing buffer containing the detergent Triton-X 100, and the C-terminus of misfolded CFTR is sensitive proteolysis due to cleavage of unassembled NBD2 (Zhang *et al.*, 1998). Therefore, the Western blots displayed in Figure 2C contain a CFTR band denoted as B*, which is most prominent in N1303K-CFTR, that migrates faster on SDS–PAGE gels than the B-band of CFTR detected in cell extracts that were immediately denatured (Figure 2A).

N1303K-CFTR does not form detergent-insoluble aggregates that partition into the pellets of centrifuged cell extracts prepared with the detergent Triton X-100. Treatment of cells for 4-h with the proteasome inhibitor bortezomib (Bort), which blocks ERAD of CFTR, did not cause a large fraction of N1303K-CFTR to form Triton X-100 insoluble aggregates that pellet on centrifugation of extracts (Figure 2C). N1303K-CFTR does not appear to be aggregation-prone, so its entrance into an off-pathway detergent-insoluble state does not account for the inability of modulators to restore its Cl- channel function.

VX-809 stabilizes N1303K-CFTR and extends its half-life severalfold. VX-809, therefore, appears to lock N1303K-CFTR in nonnative conformation that is retained in ER and resistant to degradation by ERAD. ERAD-resistant membrane proteins are degraded by an ER-associated autophagy mechanism (Buchberger, 2014), so the impact of a 6-h incubation with the lysosomal protease inhibitor chloroquine (CQ) on N1303K-CFTR accumulation and detergent solubility was evaluated in the absence or presence of VX-809 (Figure 2C). CQ treatment did not cause a change in the detergent solubility of N1303K-CFTR, but in cells treated with VX-809, the addition of CQ caused steady-state levels of N1303K-CFTR to increase. These data indicate that the accumulation of VX–809-stabilized pools of N1303K-CFTR is sensitive to inhibition of lysosomal proteolysis. In contrast, the accumulation of WT or F508del-CFTR is insensitive to the inhibition of lysosomal proteases (Houck *et al.*, 2014).

Late-stage N1303K-CFTR intermediates have the potential to engage the ER-exit site machinery and then be triaged for selective ER-phagy through interaction with complexes containing vesicle cargo selectors and coat proteins (Omari *et al.*, 2018). N1303K-CFTR localization was therefore examined relative to the cargo selector Sec24, ER-Golgi intermediate compartment-53 (ERGIC-53), the Golgi protein GM130 (Figure 2D), and Sec31 and calnexin (Supplemental Figure S2). N1303K-CFTR accumulated in the ER in zones adjacent to Sec24 but was excluded from Sec24 containing ER-exit sites. N1303K-CFTR was also not detected with ERGIC-53 or GM130. In Supplemental Figure S2, WT CFTR is shown to localize in ER-exit sites with the vesicle coat-protein Sec31, but N1303K and F508del-CFTR are excluded and instead accumulate in the ER tubules with calnexin.

The sensitivity of N1303K-CFTR accumulation to CQ suggests that the lysosome degrades at least some of its ERAD-resistant conformers. N1303K-CFTR is mobile in healthy ER membranes and is excluded from ER-exit sites. Arrested intermediates are not likely to interfere with the secretory pathway or be subjected to ERQC mechanisms that involve ER-exit sites.

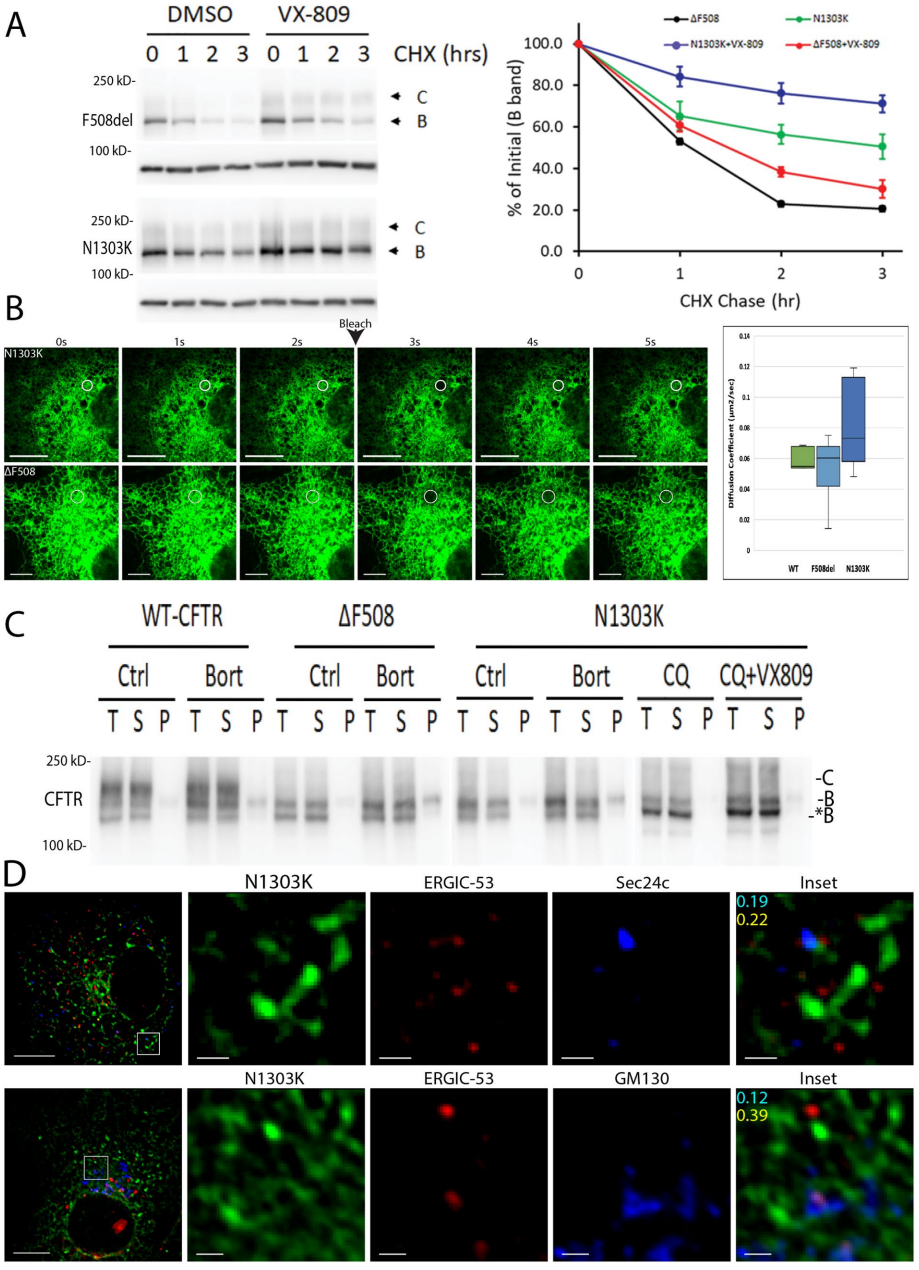

FIGURE 2: N1303K-CFTR is more stable than ΔF508 CFTR and is partially degraded by autophagy. (A). CHX chase of N1303K and ΔF508 CFTR in the absence or presence of VX-809. HEK cells were transiently transfected with N1303K and ΔF508 CFTR. At 24 h after transfection, cells were pretreated with or without 5 μM VX-809 for 2 h, followed by the addition of 100 μM CHX and incubation for the indicated time. Cell lysates in SDS–PAGE sample buffer were subjected to 7.5% SDS–PAGE and Western blot analysis with CFTR mAb 596. Protein loading was normalized by reprobing the blots with anti-tubulin antibody. Representative blots are shown on the left, with quantification normalized to tubulin shown on the right ($n = 3$). CHX chase of N1303K and ΔF508 CFTR after overnight VX-809 treatment gave similar results (not shown). Supplemental Figure S2A shows results from a chase study with WT CFTR. (B). Live-cell imaging and FRAP of EGFP-N1303K-CFTR and EGFP-F508del-CFTR that was transiently expressed in COS-7 cells and imaged with a ZEISS 880 microscope using a PMT detector. The Swarm Plot shows the diffusion coefficients for WT CFTR ($n = 5$), F508del-CFTR ($n = 8$ trials), and N1303K ($n = 10$ trials). The respective averages ± SE in $\mu M^2/s$ are 0.060 ± 0.003, 0.053 ± 0.006, and 0.084 ± 0.009. The mobility of N1303K-CFTR compared with WT or F508del-CFTR was evaluated by a Student's *t* test was found to be significantly different $P < 0.05$. (C). Fractionation of WT, F508del, and N1303K-CFTR into Triton X-100 soluble and insoluble fractions of cell extracts. In C, the SDS–PAGE resolved two bands that represent ER-localized B-form of CFTR, B and B*. In nondenaturing cell lysis buffers, the C-terminus of misfolded CFTR is sensitive to postlysis proteolysis due to cleavage of NBD2 and B* is a truncated form of B-band (D) N1303K is excluded from ER exit sites. COS-7 cells were transiently transfected with EGFP-N1303K-CFTR. 18 h after transection and 6 h prior fixation cells were treated with 15 μM CQ and 5 μM VX-809. Immunostaining was carried out on methanol-fixed cells with anti-GFP and with antibodies to endogenous ERGIC-53, Sec24C, and GM130. See Supplemental Figure S2 for images of N1303K-CFTR and F508del-CFTR in cells stained for endogenous calnexin and Sec31.

N1303K-CFTR segregates into ER subdomains with the Hsp40 JB12 or the autophagy factor LC3B

JB12 and RMA1 cooperate in selecting misfolded WT CFTR and F508del-CFTR for ERAD, and JB12 is also implicated in chaperoning ERAD-resistant pools of misfolded membrane proteins for ER-associated autophagy (Younger *et al.*, 2006; Grove *et al.*, 2011; Houck *et al.*, 2014). The mechanism for triage of misfolded membrane proteins by JB12 and Hsp70 for ERAD or ER-associated autophagy is proposed to be dictated by the conformation of misfolded intermediates; globally, misfolded, stable, or aggregated. Globally misfolded clients such as F508del-CFTR are rapidly retrotranslocated from the ER and degraded by the cytosolic proteasome. Some stable and ERAD-resistant misfolded intermediates are maintained by JB12 in a detergent-soluble conformation and triaged to ER-associated autophagy (Houck *et al.*, 2014). Misfolded intermediates that escape the action of JB12 and aggregate within the ER membrane cause cytotoxicity and do not appear to be degraded (Houck *et al.*, 2014).

We, therefore, compared the sensitivity of N1303K-CFTR and F508del-CFTR to modulation of JB12 or RMA1 activity. Modest elevation of JB12 or RMA1 activity reduced steady-state levels of N1303K-CFTR as well as F508del-CFTR. The addition of VX-809 to cell cultures 6 h prior to harvest of cells for analysis by Western blot did not protect N1303K-CFTR from the action of JB12 or RMA1. RMA1 and JB12 act synergistically during cotranslational selection of misfolded F508del-CFTR for ERAD (Younger *et al.*, 2006; Grove *et al.*, 2011). Misfolded N1303K-CFTR intermediates appear to be susceptible to the cotranslational selection by JB12 and RMA1 for ERAD. However, the steady-state levels of N1303K-CFTR are severalfold higher than those of F508del-CFTR (Supplemental Figure S3), so conformers that initiate folding and escape cotranslational recognition for ERQC may represent the ERAD-resistant forms of N1303K-CFTR.

To evaluate posttranslational interactions between JB12 and stable N1303K-CFTR intermediates, we constructed the proximity probe APEX-JB12, which contains an ER-luminal APEX (Figure 3B). APEX-JB12 labeled N1303K-CFTR in the absence or presence of VX-809, and the signal of N1303K-CFTR in streptavidin-pulldowns was larger when extracts were prepared from VX–809-treated cells. The siRNA depletion of JB12 causes an increase in the steady-state levels of N1303K-CFTR (Figure 3C). In contrast, a control depletion of an unrelated transmembrane VMP1, which regulates SERCA2B function, did not impact steady levels of N1303K-CFTR. N1303K-CFTR that escapes cotranslational selection for ERAD accumulates in JB12-containing complexes, and VX–809-stabilized N1303K-CFTR is still recognized by JB12. JB12 may act cotranslationally with RMA1 to select a fraction of misfolded N1303K-CFTR for ERAD. Yet, disruption of late steps in CFTR assembly by N1303K-CFTR creates the need for JB12 function in posttranslational ERQC of kinetically trapped N1303K-CFTR intermediates.

To evaluate the mechanism for triage of N1303K-CFTR within the ER membrane system (Kruse *et al.*, 2006; Fujita *et al.*, 2007; Houck *et al.*, 2014), we explored via fluorescence microscopy the localization of its intermediates with JB12 and endogenous LC3B. LC3B is covalently attached to the head groups of ER membrane lipids that are concentrated within ER microdomains that are associated with autophagy initiation (omegasomes) (Yla-Anttila *et al.*, 2009; Matsunaga *et al.*, 2010) (Figure 3D). As discussed below, LC3B is also a marker for autophagic vesicles and autolysosomes, but the data presented in Figure 3D focused on colocalization of N1303K-CFTR with ER-localized LC3B.

Remarkably, EGFP-N1303K-CFTR was detected in two different subsets of interconnected ER tubules containing either overexpressed WT-JB12 or endogenous LC3B (Figure 3D). The inset shows JB12 (red) in tubules with GFP-N1303K-CFTR (green) that form a perimeter around an adjacent region of the ER that is enriched in GFP-N1303K-CFTR and LC3B. Membranes containing N1303K-CFTR may therefore segregate into omegasomes where they are modified and converted into phagophores (Axe *et al.*, 2008; Yla-Anttila *et al.*, 2009; Matsunaga *et al.*, 2010; Zachari *et al.*, 2019; Ktistakis, 2020).

QPD-JB12, containing a mutation in JB12's Hsp70 binding HPD motif, binds clients but does release them because QPD-JB12 does not properly interact with Hsp70 (Grove *et al.*, 2011; Sopha *et al.*, 2017). QPD-JB12 colocalized with EGFP-N1303K-CFTR in the ER (COI of 0.69) and hindered the segregation of N1303K-CFTR into ER membranes decorated with LC3B (COI of 0.33 with WT JB12 and COI of 0.11 with QPD JB12). In cells that express QPD JB12, the mean ± SE for the COI of N1303K-CFTR and ER decorated with LC3B was 0.13 ± 0.05, which is 80% lower than the mean COI of 0.62 ± 0.03 for N1303K and LC3B in cells expressing WT JB12. This difference is statistically different at a 99% confidence level as determined by the Student's *t* test (see Figure 2 legend). Hsp70 is not required for basal autophagy, and QPD-JB12 expression does not interfere with the formation of ER-associated foci containing LC3B (Figure 3D). QPD-JB12 appears to selectively inhibit the segregation of N1303K-CFTR into ER membranes decorated with LC3B.

Endogenous JB12 was also detected via microscopy in ER microdomains with GFP-N1303K-CFTR and endogenous LC3B (Figure 3E). ER tubules containing endogenous JB12 and GFP-N1303K-CFTR intersect with tubules decorated with endogenous LC3B that extends out from ER rings. The depletion of JB12 by siRNA was accompanied by an expansion of N1303K–CFTR-containing ER membranes and the exclusion of N1303K-CFTR from LC3B-decorated ER tubular extensions. In controls, the average COI for N1303K/LC3B was 0.39 ±0.04 (average ± SE, $n = 8$), and after siJB12, the N1303K/LC3B COI was 0.13 ± 0.03 (the control and siJB12 COI values are significantly different, $P < 0.001$)

In summary, kinetically trapped intermediates of N1303K-CFTR are present in complexes containing JB12. The depletion of JB12 causes the expansion of ER domains containing N1303K-CFTR and hinders N1303K-CFTR segregation into LC3B-decorated ER tubules. JB12 depletion or inactivation does not reduce the formation of autophagic foci containing LC3B. JB12 and Hsp70 appear to be required for the selective autophagic degradation of N1303K-CFTR.

N1303K-CFTR intermediates, but not F508del-CFTR, traffic from the ER to autolysosomes

How do the N1303K-CFTR intermediates that colocalize with LC3-decorated ER-tubular extensions transit to autolysosomes (Figure 4)? To address this question, we first repeated experiments conducted with EGFP-N1303K-CFTR with untagged CFTR and demonstrated that N1303K-CFTR, but not F508del-CFTR, accumulates in autolysosomes with LC3B (Figure 4A). Three-color imaging was also employed to show that EGFP-N1303K-CFTR and LC3B-positive puncta also contain LAMP1/2 and are, in fact, autolysosomes (Figure 4B). In these experiments, cells were pretreated for 6 h with VX-809 to stabilize N1303K-CFTR intermediates and bafilomycin A1 to suppress degradation of N1303K-CFTR in autolysosomes. These conditions enhance the visualization of endogenous LC3B and LAMP1/2 with N1303K-CFTR in autolysosomes.

Autophagic degradation of some misfolded ER luminal proteins occurs via a process involving receptor-mediated vesicular transport and therefore is not regulated by autophagy initiation kinases (Forrester *et al.*, 2019). If the movement of N1303K-CFTR from the ER to the lysosomes were to occur via a similar pathway, it would also be independent of autophagy initiation kinases. It would also be predicted to require the ER-phagy receptor FAM134B (Forrester *et al.*, 2019; Wilkinson, 2019, #6308).

To define features of the ER-associated autophagy pathway N1303K-CFTR, we evaluated the requirement of autophagy initiation kinases and ER-phagy receptors in N1303K-CFTR degradation (Figure 4B and Supplemental Table S1). The VPS34 inhibitor PIK-III blocked the entry of GFP-N1303K-CFTR into autolysosomes containing LAMP1 (Figure 4B) and did so under conditions where conversion of LC3B-I to LC3B-II was abolished (Supplemental Figure S3B). Likewise, siRNA of Beclin-1, treatment of cells with a ULK1 inhibitor and overexpression of a dominant-negative form of ULK1 also blocked the transit of GFP-N1303K-CFTR from the ER to autolysosomes (Supplemental Table S1). In addition, depletion of FAM134B via siRNA or CRISPER CAS-9 did not cause the accumulation of N1303K-CFTR in the ER or reduce trafficking of N1303K-CFTR to autolysosomes (Supplemental Table S1).

Consistent with the requirement for JB12 in the colocalization of N1303K-CFTR in the ER with LC3B (Figure 3E), siRNA of JB12 diminished the trafficking of N1303K-CFTR to LAMP1/2-positive autolysosomes (Figure 4C). The COI for N1303K-CFTR/LAMP1/2 is 0.38 ± 0.03 ($N = 8$, average ± SE). siRNA depletion of JB12 causes an increase in the ER pools of N1303K-CFTR and a significant reduction in the N1303K-CFTR/LAMP1/2 COI to 0.16 ± 0.03 ($N = 8$). This reduction is significantly different from the control ($P < 0.001$). SiRNA of JB12 does not completely block colocalization of N1303K-CFTR with LAMP1/2. Yet, this is to be expected because, in the absence of JB12, lysosomes remain associated with ER tubules containing N1303K-CFTR.

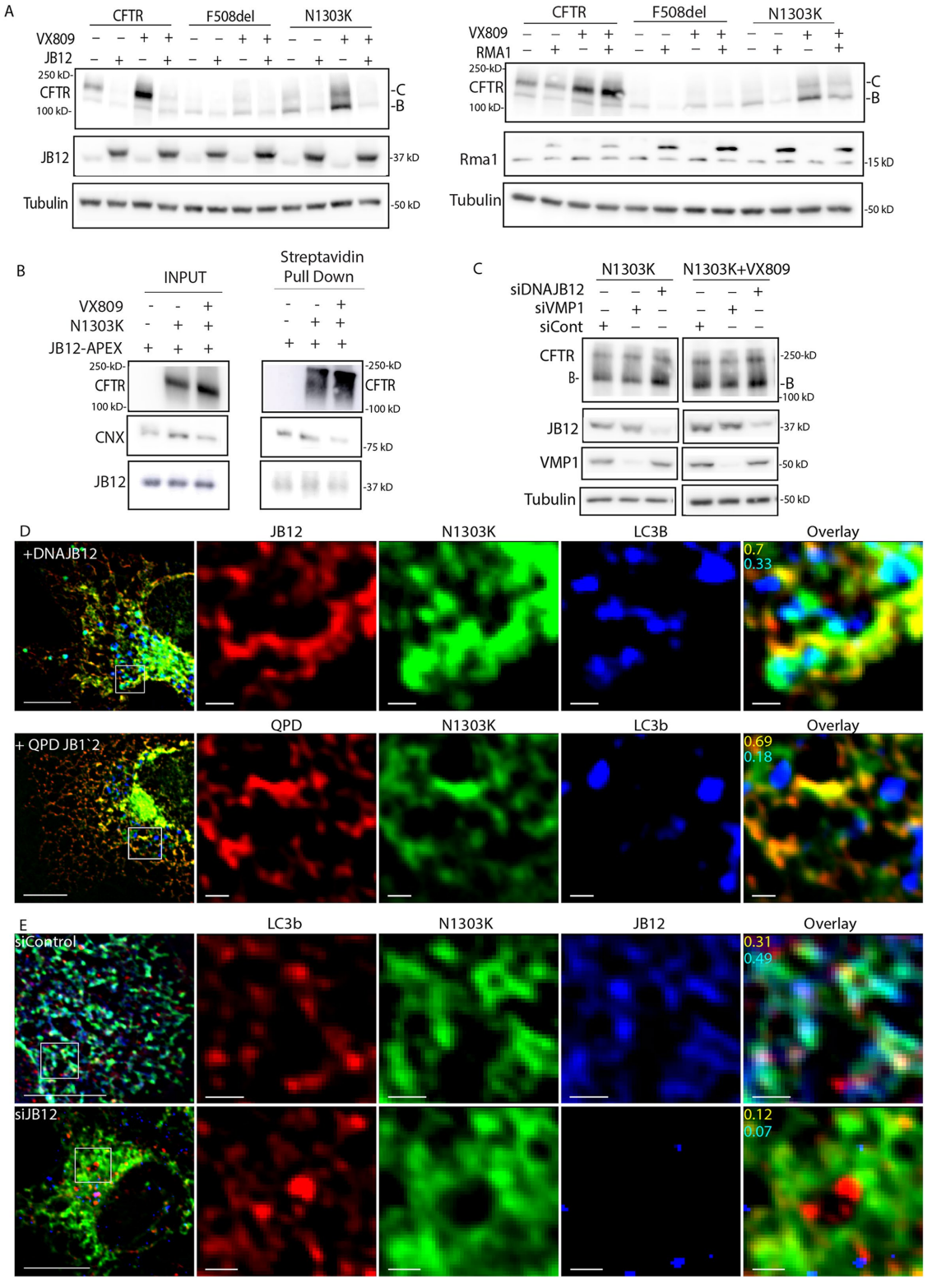

FIGURE 3: N130K-CFTR is sensitive to elevation of JB12 and RMA1/RNF5 and accumulates in ER tubules with JB12 or membranes that exclude JB12 and contain LC3B. (A) Changes in steady-state levels of CFTR, F508del-CFTR, and N1303K-CFTR in the absence or presence of VX-809 (5 μM) that are caused by the elevation of JB12 or RMA1/RNF5. Indicated forms of CFTR were expressed in the absence or presence of VX-809 that was added to cell cultures 6 h prior to harvest and analysis by Western blot. Western blots in the middle panels show levels of overexpressed JB12 (50 ng of pCDNA3-DNAJB12) or RMA1/RNF5 (100 ng of pCDNA-RMA1/RNF5) relative to endogenous pools. (B) Proximity labeling of N1303K-CFTR by JB12-APEX in the absence or presence of VX-809. JB12-APEX, which contains an APEX domain localized in the ER lumen, that was coexpressed with N1303K-CFTR in the absence or presence of VX-809. Cells were incubated with hydrogen peroxide and biotin-phenol and modified adducts were then isolated from cell extracts

In summary, we have demonstrated that arrested N1303K-CFTR requires the activity of canonical autophagy initiation kinases and JB12 to accumulate within LC3B-decorated ER microdomains and LAMP1/2 in autolysosomes. N1303K-CFTR is not detected within ER-exit sites, and a role for FAM134B or additional ER-phagy receptors such as TEX264, CCPG1, or SEC62 in N1303K-CFTR accumulation within autolysosomes could not be demonstrated (Supplemental Table S1). The autophagic mechanism for degradation of detergent-soluble intermediates of N1303K-CFTR is therefore distinct from selective ER-phagy of ERAD-resistant conformers of secretory proteins and stress-damaged ER membranes (Omari *et al.*, 2018; Forrester *et al.*, 2019; Wilkinson, 2019).

ER membranes enriched in N1303K-CFTR protrude from WIPI1 rings

The route taken by N1303K-CFTR from the tubular-ER to the autolysosome was explored by visualizing its association with the omegasome factors DFCP1 and WIPI1, and LAMP1. The VPS34 kinase complex produces pools of inositol-3-phosphate head groups on ER membrane lipids that are bound by cytosolic DFCP1 and WIPI1, which facilitate downstream reactions in phagophore formation involving LC3 conjugation and autophagosome biogenesis (Tooze and Yoshimori, 2010). In live COS-7 cells, GFP-N1303K-CFTR was present in ER tubules that feed into ER sheets that were decorated with RFP-DFCP1 (Figure 5A and Supplemental Figure S4). The EGFP-N1303K/mCherry-DFCP1 foci attached to multiple interconnected ER tubules, around 1 μM wide, and protruded into ringlike ER microdomains (Figure 5A). Similarly, in fixed COS7 cells, EGFP-N1303K-CFTR, but not F508del-CFTR, is detected within ringlike domains that are decorated mCherry-WIPI1 (Figure 5B and Supplemental Figure S4). Interestingly, ER tubes containing EGFP-N1303K-CFTR enter WIPI1-decorated membranes at locations that contain FIP200, a ULK1 localization factor. ER membranes containing N1303K-CFTR of different diameters are observed to extend from FIP200-enriched surfaces of WIPI-rings, and these membranes appear to be phagophores. Use of STED microscopy to image GFP-N1303K-CFTR, LC3-mCherry, and BFP-LAMP1 in live cells enabled visualization of GFP-N1303K and LC3 containing foci that interact with autolysosomes containing BFP-LAMP2 (Figure 5C). ER tubules containing N1303K-CFTR that are decorated with LC3B are detected in contact with an ER-docked lysosome. Small foci containing LC3 and N1303K-CFTR are also detected in the surface where the lysosomes have docked to the ER.

Data in Figure 5 are interpreted to suggest that ER tubules containing N1303K-CFTR are converted to phagophores within WIPI-rings in a process involving FIP200. Lysosome binding to LC3B-decorated ER tubules that contain N1303K-CFTR could couple the budding of N1303K-CFTR containing autophagosomes from omegasomes to fusion with docked lysosomes. These interpretations are consistent with results from ultrathin sectioning and electron microscopic studies showing connections between ER tubules and phagophores formed in starved cells (Yla-Anttila *et al.*, 2009) and observations that FIP200 recruits ULK1 to membranes to initiate focal activation of selective autophagy (Vargas *et al.*, 2019).

The conformation of CFTR intermediates controls triage for ERAD versus ER-associated autophagy

To understand why N1303K-CFTR is selected for ER-associated autophagy, we investigated the role played by the conformation of kinetically trapped intermediates (Figure 6). The conformation of N1303K-CFTR intermediates was probed with a cysteine (Cys) pair cross-linking assay that monitors the formation of contacts between NBD1 or NBD2 with different CLs identified in high-resolution models of CFTR structure (Serohijos *et al.*, 2008) (Figure 6, A–C). Cys pairs were introduced at CL/NBD interfaces in Cys-less CFTR with or without N1303K, and cross-linking was conducted to evaluate the folding of CFTR to a conformation that contains the indicated domain interfaces (He *et al.*, 2013). When a Cys pair was introduced at the CL2/NBD2 interface at amino acid residues C276C/Y1307C, cross-linking of CFTR was detected after treatment of cells with methanethiosulfonate (MTS) disulfide bond cross-linkers of different spacer arm lengths, M3M and M8M (Figure 6C, lanes 2 and 3, marked with X). VX-809 increased signals that report on the CL2/NBD2 interface within WT-CFTR, accumulating in the low mobility C-form (Figure 6C, lanes 5 and 6). However, in the absence or presence of VX-809, no cross-linked band was detected in N1303K-CFTR that reports on the CL2/NBD2 interface (Figure 6C, lanes 7–12).

The Cys pair at amino acid residues E543C/T1057C, in NBD1 and CL4, respectively, was acted on by both MTS cross-linkers M3M and M8M to generate a lower mobility C-form of CFTR (Figure 6D, lanes 2 and 3). The introduction of N1303K into this reporter prevented the C-form of CFTR (Figure 5D, lane 7). Still, a faint cross-linked band was detected slightly above the C-band's location and is seen in extracts of cells treated with M3M and M8M (Figure 6D, lanes 8 and 9, marked with an X'). VX-809 treatment increased the B-form N1303K-CFTR (Figure 6D, lane 10) and the amount of band X' (Figure 6D, lanes 11 and 12). VX-809 also restored the interface between CL3/NBD1 in N1303K-CFTR, as shown with the cross-linking of E543C/T966C marked with X' (Figure 6E).

Subdomains of N1303K-CFTR assemble into a conformation that has features of folded WT CFTR, but folding steps involving NBD2 are defective and resistant to modulation by VX-809. The combined folding of N1303K-CFTR's N-terminal domains and

by streptavidin-pull downs and detected by Western-blot with indicated antibodies. (C) Analysis of the localization of GFP-N1303K-CFTR in the ER relative to JB12 or RMA1/RNF5. N1303K-CFTR was expressed in COS-7 cells in the absence or presence of JB12 (expressed 50 ng of pCDNA3). Cells were fixed with methanol and stained for JB12 or endogenous LC3. Immunofluorescence images were collected with an Olympus IX-81 with CellSens software and processed with ICY. (D) Localization of overexpressed FLAG-DNAJB12 or FLAG-QPD-DNAJB12 with EGFP-N1303K-CFTR in COS-7 cells. Cells were fixed in methanol at –20°C for 5 min, then blocked for 1 h at ambient temperature with blocking buffer (3% BSA in phosphate-buffered solution), followed by primary and secondary antibody labeling. After washes with blocking buffer, coverslips were mounted using ProLong Diamond with DAPI mounting solution and sealed immediately with nail polish. (E) Impact of JB12 siRNA on EGFP-N1303K association with endogenous LC3B in CoS-7 cells. Cells were transiently transfected (Effectene) with GFP-N1303K and then fixed (using same procedure as in D). In cells that expressed JB12, the mean COI ± SE for the N1303K-CFTR/LC3B COI was 0.62 ± 0.03 ($N = 5$) vs. 0.11 ± 0.05 ($N = 7$) in QPD–JB12-expressing cells. COIs for the SiRNA experiments are presented in the text. The COIs are significantly different with a Student's *t* test, $P < 0.001$.

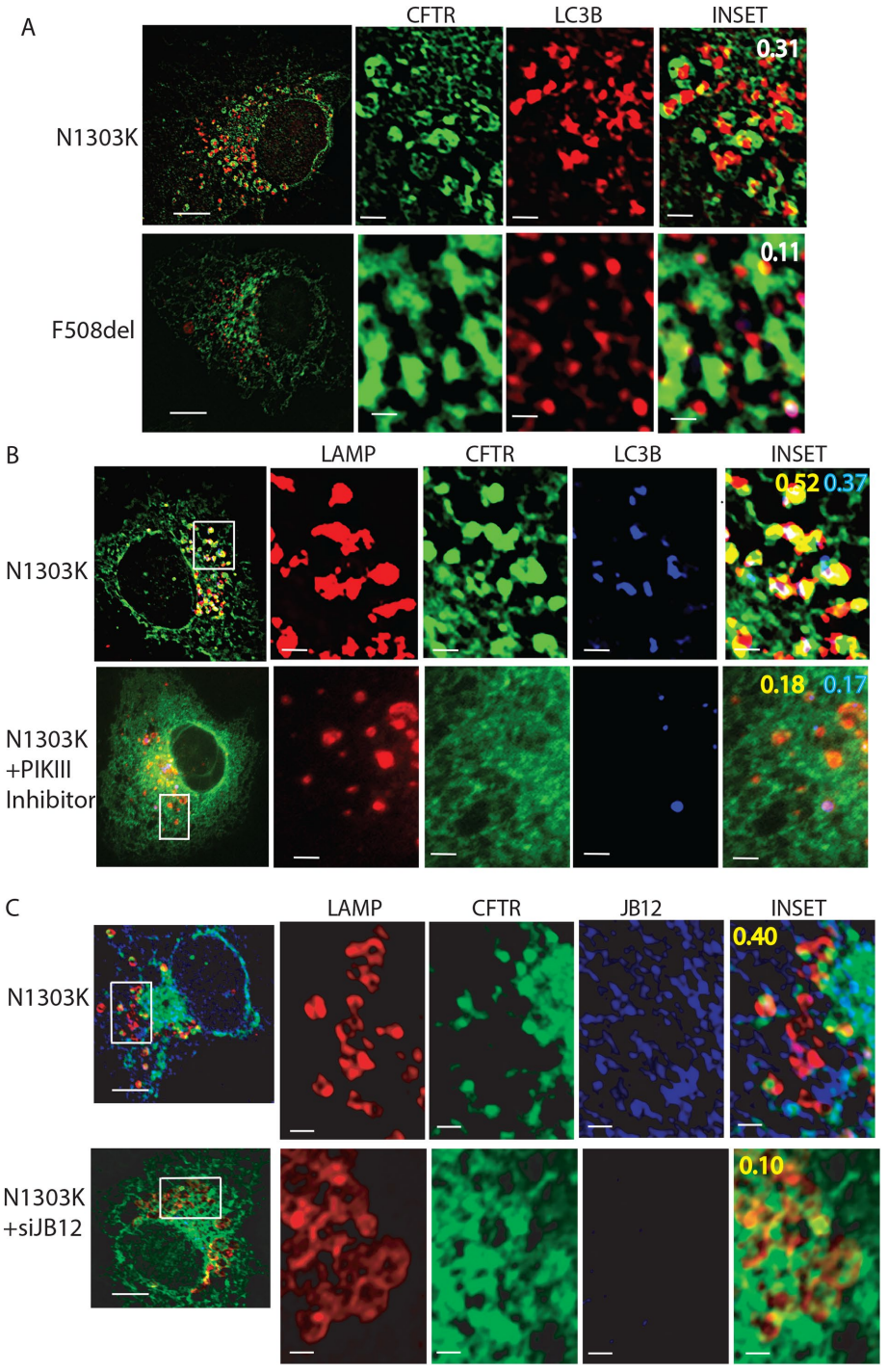

FIGURE 4: JB12 is necessary for traffic of N1303K-CFTR from the ER to Autolysosome. (A) Localization in COS-7 cells of untagged N1303K-CFTR, but not F508del-CFTR, in foci with endogenous LC3B. (B) Localization of EGFP-N1303K-CFTR in autolysosomes with endogenous LAMP1 and LC3B is sensitive to PI3K-III, an inhibitor of the autophagy initiation kinase, VPS34. (C) Depletion of JB12 from COS-7 cells by siRNA reduces movement of N1303K-CFTR from the ER to LAMP1 positive foci. JB12 levels were reduced via siRNA and 18 h later cells were transfected with GFP-N1303K-CFTR. Cells were fixed 18 h after introduction of GFP-N1303K-CFTR and stained for the indicated endogenous proteins. Cells were treated with VX-809 and bafilomycin as described from Figure 3 and in *Materials and Methods*. Immunofluorescence images were collected with an Olympus IX-81 with CellSens software and processed with ICY. Results obtained using antibodies to LAMP1 and LAMP2 were similar, so they were used interchangeably as lysosome markers.

failure to N1303K-NBD2 fold could cause the accumulation of kinetically trapped intermediates.

Impacts of N1303K-CFTR's conformation on triage decisions

To test the model proposed for conformation-dependent triage of CFTR intermediates, we developed a CFTR reporter that is conditionally sorted to autolysosomes in the presence of VX-809 (Figure 7A). The disease-causing mutation P67L located in the N-terminus causes global misfolding and degradation of P67L CFTR by ERAD, and VX-809 completely restores the folding and function of P67L CFTR (Ren *et al.*, 2013). P67L was therefore introduced into N1303K-CFTR to create P67L-N1303K-CFTR. It was then asked: 1) what is the effect of P67L on the triage of N1303K-CFTR to ER-associated autophagy? 2) Does stabilization of N-terminal domains by VX-809 cause P67L-N1303K-CFTR to be triaged similar to N1303K-CFTR? P67L-N1303K-CFTR intermediates exhibited a short half-life and were not detected in autolysosomes (Figure 7, A and B). Treatment with VX-809 restored P67L-CFTR folding and accumulation in the C-form, and in parallel incubations, we observed VX-809 increase the stability of P67L-N1303K-CFTR intermediates, which was associated with the accumulation of VX–809-stabilized P67L-N1303K-CFTR in autolysosomes (Figure 7, A and B). These data demonstrate that the biochemical stability of CFTR intermediates strongly influences the triage of misfolded CFTR to ER-associated autophagy.

DISCUSSION

We report that the mutation N1303K in NBD2 arrests CFTR folding at a late stage and causes kinetically trapped intermediates to accumulate in the ER. N1303K-CFTR intermediates are chaperoned by JB12 and Hsp70 and triaged in a conformation-specific manner for degradation by ERAD or ER-associated-autophagy. Data presented suggest that globally misfolded CFTR is degraded by ERAD, whereas biochemically stable intermediates are selected for ER-associated-autophagy. N1303K-CFTR intermediates have long 3-h half-lives, are soluble in nonionic detergent, are mobile in the ER tubular network, and contain cross-linkable domain interfaces that are detected in folded CFTR. N1303K-CFTR intermediates are stabilized by VX-809, but stabilized N1303K-CFTR does not escape the ER and remains associated with JB12 and additional PQC factors. Disruption of early steps

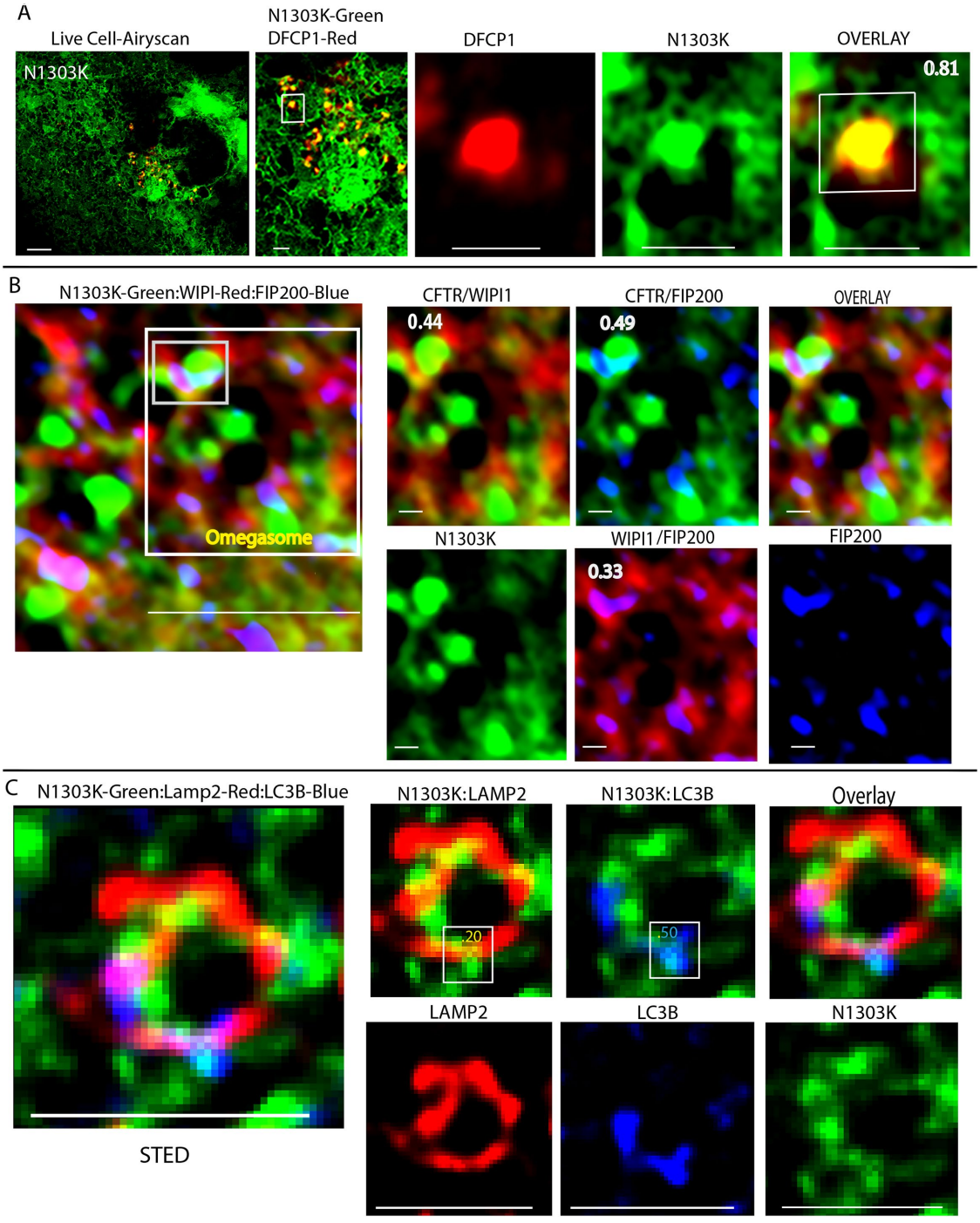

FIGURE 5: N1303K-CFTR intermediates, but not F508del-CFTR, are detected by fluorescence microscopy with autophagy initiation machinery during sorting within the ER and trafficking to autolysosome. (A) In live COS-7 cells that did not receive chemical treatment EFGP-N1303K-CFTR is detected in ER tubules that associate with membrane that are decorated with the autophagy initiation factor mCherry-DFCP1. (B) In fixed COS-7 cells that were treated with bafilomycin A1 6 h and VX-809 (5 mM) for 16 h N1303K-CFTR is detected in association with ER membranes that are decorated with mCherry-WIPI1 and endogenous FIP200. (C) Superresolution analysis of COS-7 cells showing the associations between N1303K-CFTR, endogenous LAMP2 and LC3B. Panels in A display images of live COS-7 cells expressing EGFP-N1303K-CFTR and RFP-WIPI taken on a ZEISS 880 microscope with AIRYSCAN. Panels in B display images of fixed COS-7 cells expressing GFP-N1303K-CFTR and the indicated mCherry-tagged or endogenous marker proteins obtained with an Olympus IX-81. In images displayed in C were obtained at superresolution with a Lecia STED Microscope in fixed cells and depict localization EGFP-N1303K-CFTR in relation to endogenous LAMP2 and LC3B (see the *Materials and Methods* for details). Images were deconvoluted with CellSens and COIs were calculated and processed with ICY and Adobe Photoshop. COIs shown in panels are for EGFP-N1303K-CFTR/LAMP2 or EGFP- N1303K-CFTR/LC3B for the boxed areas of panels. The scale bars in A are 1 μM. In B the scale bar for the composite image is 10 μM and 1 μM in the panels showing signals in split channels. In C the scale bar for the composite image is 1 μM.

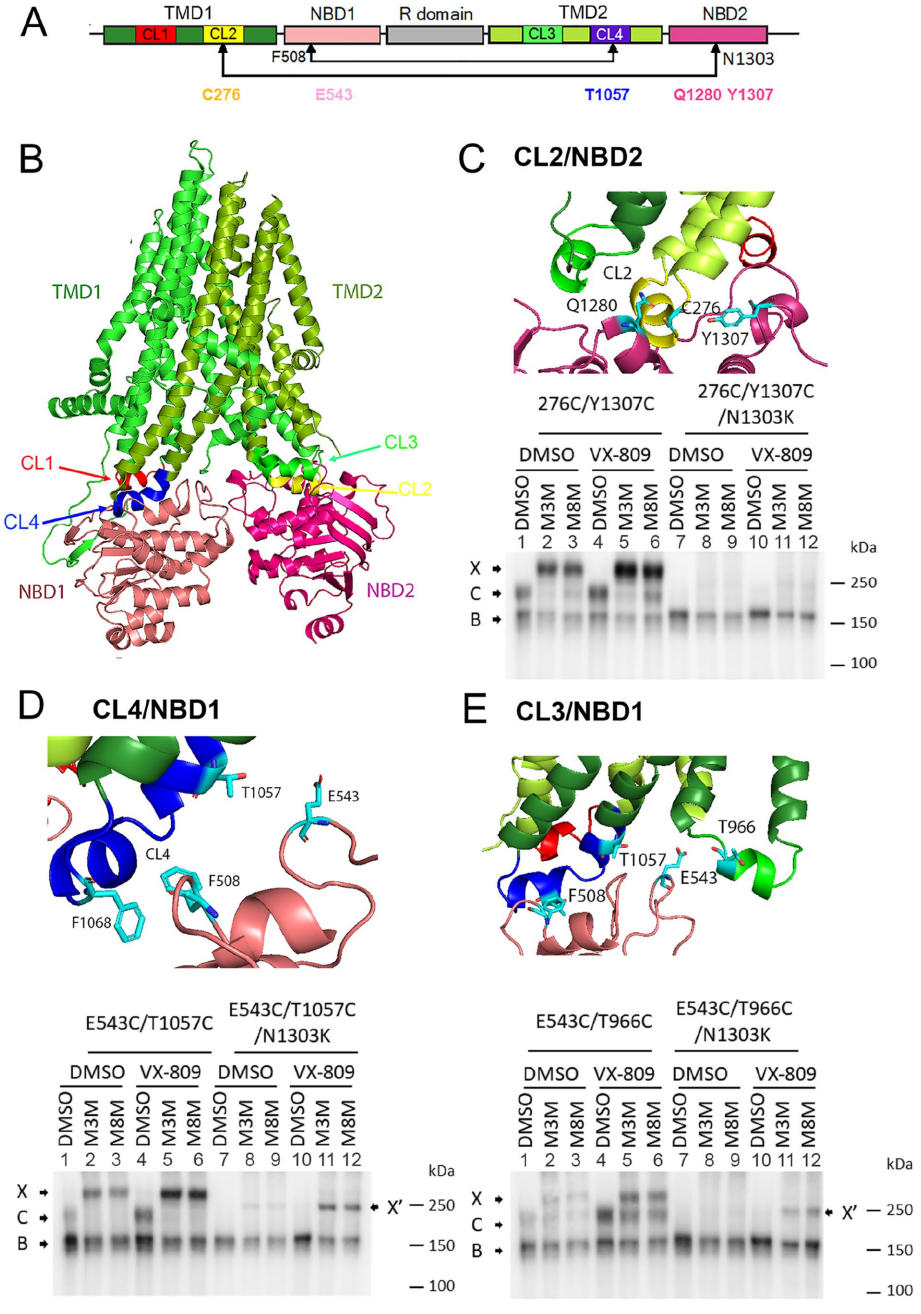

FIGURE 6: N1303K-CFTR folded to a conformation that contains native-like domain:domain contacts between NBD1 and ICL4, but native-like assembly of NBD2 is not detected. (A). Model for domain structure of CFTR containing two nucleotide-binding domains (NBD1 and NBD2), two membrane-spanning domains (MSD1 and MSD2), and a regulatory region (R domain). Each MSD contains two CLs that form interfaces with the NBDs. F508 in NBD1, N1303 in NBD2, and residues mutated to Cys are marked. (B) The three-dimensional structure of human CFTR (5UAK) with major domains and CLs labeled. (C–E). Cross-linking of Cys pairs introduced at different CL/NBD interfaces. HEK293 cells were transiently transfected with Cys-less CFTR or Cys-less N1303K-CFTR with Cys pairs E543C/T1057C introduced at CL4/NBD1 interface (B), E543C/T966C at CL3/NBD1 interface (C), and 276C/Y1307C at CL2/NBD2 interface (D), respectively. At 24 h after transfection, cells were treated with 3 μM VX-809 for 24 h at 27°C. Cells were harvested and resuspended in PBS and incubated with 200 μM M3M, M8M, or an equal amount of DMSO as vehicle control. Cell lysates in SDS–PAGE sample buffer without DTT were subjected to 7.5% SDS–PAGE and Western blot analysis with mAb 596. C, mature complex-glycosylated CFTR; B, immature core-glycosylated CFTR; X, cross-linked mature CFTR; X′, cross-linked immature CFTR. Additional cross-linking experiments are presented in the supplement.

in CFTR folding to cause global misfolding of N1303K-CFTR via the introduction of the P67L mutation reduces the half-life of N1303K-CFTR, and P67L-N1303K-CFTR is not detected in the autophagy system. VX-809 stabilizes P67L-N1303K-CFTR intermediates causing them to be triaged to ERQC-autophagy. Data reported on N1303K-CFTR support the concept that in energized and biosynthetically active ER membranes, non-toxic intermediates of misfolded membrane proteins are selectively triaged based on their conformation for proteasomal or lysosomal degradation.

CFTR degradation intermediates are now grouped with an expanding collection of secretory and membrane proteins that misfold and accumulate in ERAD-sensitive or ERAD-resistant conformations (Buchberger, 2014; Houck *et al.*, 2014). ERAD requires that misfolded luminal or membrane proteins be unfolded and retrotranslocated to the cytosol where they are translocated into the narrow opening of the proteasome proteolytic chamber. In cases in which nascent secretory proteins misfold in the ER lumen and adopt a retrotranslocation-resistant conformation, the trapped intermediates interact with complexes containing ER-phagy receptors before selective ER-phagy (Fregno and Molinari, 2018). We extensively evaluated the role of selective ER-phagy in the conformation-dependent triage of N1303K-CFTR. We did not identify an ER-phagy receptor or soluble autophagy receptor necessary for its conformation-dependent sorting and traffic to autolysosome (Supplemental Table S1). Since there are a large number of LIR-containing proteins implicated in selective ER-phagy and selective autophagy, it could be that functional redundancy complicates the interpretation of siRNA and CRISPR/Cas9 loss of function experiments. However, we combined gene inactivation with imaging analysis and biochemical studies and were unable to observe physical or functional interactions that were suggestive of a role for soluble or ER membrane associated autophagy receptors in ERQC of N1303K-CFTR.

In contrast to results reported with N1303K-CFTR, aggregates of ER-luminal alpha-1-antitrypsin and large assemblies of misfolded collagen are cleared from the ER by a selective ER-phagy process involving FAM134B and the ER exit site protein Sec31 (Omari *et al.*, 2018; Forrester *et al.*, 2019). N1303K-CFTR is excluded from ER exits and does not colocalize with Sec 24 or Sec31, so it is not likely to be degraded by the pathway used for selective ER autophagy of

misfolded collagen. The chaperone calnexin binds selective ER-phagy clients in the lumen and functions in a complex with FAM134B to target them for selective ER-phagy. CFTR is a calnexin client, and calnexin facilitates assembly reactions involving C-terminal regions of CFTR, but a role for FAM134B in the degradation of N1303K-CFTR could not be demonstrated (Supplemental Table S1). These results may be observed because polytopic membrane proteins expose ubiquitinated surfaces in the cytosol when they fail to fold correctly. N1303K-CFTR, like other misfolded forms of CFTR, is ubiquitinated, which could permit cytosolic ubiquitin chain-binding autophagy receptors to usurp requirements for ER-phagy receptors. However, we could not demonstrate a role for p62, NBR1, FKBP8, or Tollip in the conformation-dependent sorting of misfolded membrane proteins to the autophagy initiation sites where ER tubules that contain N1303K-CFTR associate with WIPI1-rings (Supplemental Table S1). Mechanisms for the conformation-dependent selection of misfolded and detergent-soluble forms of CFTR for selective ER-associated autophagy, therefore, appear different than those demonstrated for ERAD-resistant luminal aggregates and aggregates of cytosolic proteins.

Triage of nascent CFTR between folding and degradation is mediated by JB12, Hsp70, and ERQC-E3 ligases such as RMA1/RNF5 and CHIP (Meacham *et al.*, 1999, 2001; Younger *et al.*, 2006; Grove *et al.*, 2011). N1303K-CFTR is present in complexes with JB12 and Hsp70, and siRNA depletion of JB12 hinders degradation of N130K-CFTR and blocks the accumulation of N1303K-CFTR in autolysosomes. The overexpression of dominant-negative QPD JB12 also prevents N1303K-CFTR from being degraded by ERAD or autophagy. QPD-JB12 can bind clients, but cannot interact with Hsp70, so QPD-JB12 can bind but fails to efficiently release clients (Grove *et al.*, 2011). JB12 is not required for basal autophagy, so a functional interaction of JB12 and Hsp70 appears needed to deliver N1303K-CFTR to the ER's autophagy machinery. JB12 is detected in complexes with Beclin-1, and complex formation between

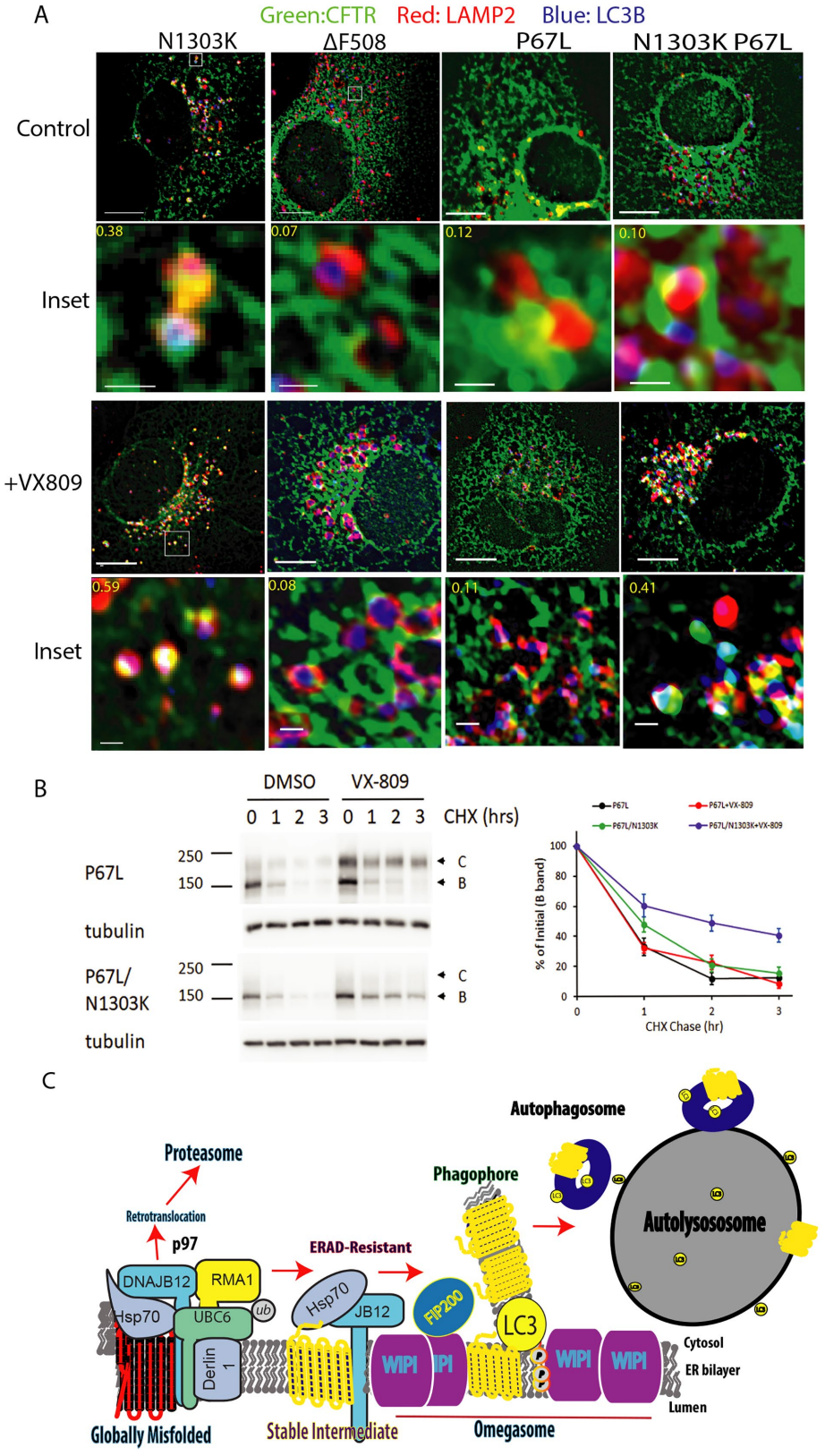

FIGURE 7: Introduction of N1303K in P67L CFTR renders it to be recognized by autophagy machinery after VX-809 treatment (A). P67L/N1303L CFTR as a model to test conformation specific triage of CFTR degradation. COS-7 cells were transfected with various EGFP-tagged mutant CFTR. Cells were treated overnight with VX-809 before bafilomycin A1 treatment for 6 h. Immunostaining was carried out with anti-LAMP2 (shown in red) and anti-LC3B (shown in blue) antibodies. (B) CHX chase of P67L and P67L/N1303K-CFTR. HEK cells transfected with P67L CFTR or P67L/N1303K-CFTR and CHX chase was carried out as described in Figure 2A figure legend. (C) Schematic summarizing data presented that describe steps in the pathway for sorting of stable N1303K-CFTR intermediates from the ER to autolysosomes.

JB12 and Beclin-1 is stimulated by ERQC-autophagy clients (Houck *et al.*, 2014). Therefore, stable client binding to JB12 could trigger the focal nucleation of autophagy-initiation machinery (Joo *et al.*, 2011; Pickles *et al.*, 2018) and facilitate the observed sorting of ER tubules containing ERAD-resistant N1303K-CFTR to omegasomes. However, additional studies are required to determine the mechanism by which JB12 and Hsp70 assist in the sorting of stable degradation intermediates of membrane proteins to the autophagy initiation sites within the ER.

To define the pathway for N1303K-CFTR intermediates from the ER to the autolysosome, we carried out a combination of fixed and live-cell imaging at normal and superresolution. In particular, we sought to determine if N1303K-CFTR entered autolysosomes via an ER–phagy-like mechanism, in which ER subdomains containing N1303K-CFTR are consumed by phagophores versus a focal mechanism involving entry of N1303K-CFTR into membranes for ER-derived autolysosomes (Houck *et al.*, 2014). To test the latter possibility, we evaluated the association of ER membrane containing N1303K-CFTR or F508del-CFTR with autophagy initiation site machinery (WIPI1, LC3B, FIP200) that localize within omegasomes and phagophores. ER membranes enriched in N1303K-CFTR and F508del-CFTR (Supplemental Figure S4) were detected on the perimeter of WIPI1-decorated ER membranes, but only N1303K-CFTR was detected in ER-associated membranes which were decorated with the phagophore marker LC3B. Likewise, N1303K-CFTR was also seen in WIPI1-enriched foci with the ULK1 subunit FIP200. In contrast, JB12 was excluded from ER tubules that are decorated with LC3b and/or associate with WIPI1 and FIP200. It was common for LAMP1-enriched lysosomes to be detected in association with ER membranes containing N1303K-CFTR that extend from the ER surface. There were also N1303K-CFTR and LC3B-containing foci in the 50-nm size range that were sandwiched between the ER and docked lysosomes. Such foci appear to represent autophagosomes in the act of docking with lysosomes. These imaging data are consistent with the concept of ER-associated-autophagy involving the focal activation of selective autophagy in response to the accumulation of ERAD-resistant intermediates of N1303K-CFTR.

N1303K-CFTR is the second most common missense mutation that causes misfolding of CFTR that gives rise to CF, and it was hoped that folding modulators developed to restore the F508del-CFTR function could also fix the function of N1303K-CFTR function. The class I modulator VX-809 does increase the accumulation of N1303K-CFTR, but not proper folding. Treatment with VX-809 alone, or in combination with the tool compounds in the Class II modulator family, or VX-441, which is used in combination with class I modulators clinically, does not restore N1303K-CFTR function in heterozygous or homozygous native human airways cells from CF patients (Veit *et al.*, 2020). However, we were able to fix the folding of a small fraction of N1303K-CFTR in cells that are cultured at low temperatures. Reconstituted N1303K-CFTR channels isolated from the plasma membranes of cells cultured at low temperature and assayed over a range of temperatures had the same conductance as WT CFTR. Rescued N1303K-CFTR channels were, however, thermodynamically unstable with a dramatically lower P_o than WT CFTR. Notably, the CFTR channel potentiator VX-770 was found to enhance the P_o of N1303K-CFTR at temperatures between 20 and 37°C, but rescued channels remained unstable.

Folding/assembly of NBD2 is a slow step in CFTR biogenesis that involves cooperative conformational changes that result from dimerization of NBD2 with NBD1 and reorientation of transmembrane spans and CLs (Kirk and Wang, 2011). Defects in the folding of N1303K-NBD2 could block the folding progression of partially assembled intermediates for several reasons. Class I and Class II modulators were developed to overcome defects in F508del-NBD1 folding/assembly, and they are also able to suppress functional defects in a subset of non-F508del-CFTR mutants. Yet, rare CFTR alleles that respond to Trikaftor have common biogenic defects similar to those caused by F508del (Middleton *et al.*, 2019). Such defects are suppressed allosterically by stabilizing N-terminal regions of CFTR and promoting intramolecular domain: domain assembly reactions involving F508del-NBD1 (Ren *et al.*, 2013; Veit *et al.*, 2016). Clinically relevant restoration of the N1303K-CFTR function might be achievable through the development of modulators that rescue defects in NBD2 misfolding and/or assembly.

MATERIALS AND METHODS

Reagents and antibodies

Reagents and antibodies were purchased from the following suppliers: HRP–conjugated goat anti-mouse IgG (31430) and goat anti-rabbit IgG (31461); Alex Fluor 488 goat anti-mouse IgG (A11029), Texas Red goat anti-mouse IgG (T-862), and goat anti-rabbit IgG (T-2767); and Alexa Fluor Plus 647 goat anti-mouse IgG (A32728) and goat anti-rabbit IgG (A32733) are from Thermo Fisher Scientific. Anti-beclin-1 (NB500-249), anti-FAM134B (NBP2-55248), and anti-Sec62 (NBP1-84045) are from Novus Biologicals. Anti-calnexin (C4731), anti-HA (H9658), anti-LC3B (L7543), anti-Myc (C3956), and anti-tubulin (T-9026) are from Sigma-Aldrich. Anti-ERGIC53 (ALX-804-602) is from Enzo Life Sciences. Anti-GABARAP+L1+L2 (ab109364) and anti-GM130 (ab52649) are from Abcam. Anti-LAMP2 (555803) and anti-Sec31A (612351) are from BD Pharmingen. Anti-p62 (H00008878-M0162) is from Abnova. Anti-VMP1 (12978s) is from Cell Signaling. DC Protein Assay (500-0119) and Clarity Western ECL Substrate (170-5061) are from Bio-Rad. Effectene Transfection Reagent (301427) is from Qiagen. Lipofectamine RNAiMAX Reagent (100014472) is from Thermo Fisher Scientific. MTS cross-linking reagents M3M (1,3-propanediyl bis-MTS) and M8M (1,5-pentanediyl bis-MTS) are from Toronto Research Chemicals. ProLong Diamond antifade mountant without (P36970) or with DAPI (P36971) is from Thermo Fisher Scientific.

Cell culture and transfection

African green monkey kidney cells (COS-7 ATCC CRL-1651), human embryonic kidney cells (HEK293, ATCC CRL-1573), and baby hamster kidney cells (BHK-21, ATCC CCL-10) were cultured in DMEM supplemented with 10% fetal bovine serum (Sigma-Aldrich, St. Louis, MO) and 10 U/ml penicillin and 10 µg/ml streptomycin (GIBCO, Carlsbad, CA) at 37°C, 5% CO_2. Human lung tissue was procured under the University of North Carolina Office of Research Ethics Biomedical Institutional Review Board Approved Protocol No. 03–1396. Primary HBE cells were harvested and cultured using established procedures previously described in detail (Fulcher *et al.*, 2005).

Plasmid transfections in cell lines were performed using Effectene Transfection Reagent following the product instruction. For knockdown experiments, all siRNAs were purchased from Thermo Fisher Scientific. For some target genes, two siRNAs to the same target gene were used to increase knockdown efficiency. COS-7 or HEK293 cells that were seeded into a 6-well plate at 3×10^5 cells/well for 20 h were transfected at five pmol per well of siRNA with Lipofectamine RNAiMAX. Twenty hours posttransfection, the cells were split again to the appropriate density for transfection of plasmids using Effectene Transfection Reagent.

Protein sample preparation for SDS–PAGE and Western blotting

COS-7 cells or HEK293 cells were harvested from plates with citric saline (135 mM KCl, 15 mM sodium citrate), and cell pellets were resuspended in phosphate-buffered saline (PBS)-T lysis solution (1% [vol/vol] Triton X-100 in PBS) supplemented with 1 mM phenylmethylsulfonyl fluoride, 1× complete protease inhibitor cocktail (Roche, Basel, Switzerland); 2× Laemmli sample buffer without reducing agent was added, and the total lysates were homogenized by sonication. Protein concentrations were measured using detergent-compatible DC Protein Assay Reagent, and 50 mM dithiothreitol (DTT) was added before samples were resolved by SDS–PAGE and proceeded to Western blot analysis. Protein signal was detected by Clarity western ECL substrate and visualized by LAS680 imager (GE Life Sciences, Pittsburgh, PA). Images were analyzed by ImageJ (National Institutes of Health [NIH]) and quantified with ImageQuant (GE Life Sciences, Pittsburgh, PA).

Coimmunoprecipitation assay

HEK293 or COS-7 cell lysates in PBST solution (1% Triton X-100 in PBS) were centrifuged at 100,000 × *g* at 4°C for 10 min to remove any insoluble fraction. Protein concentrations were measured using DC Protein Assay, and samples of an equal amount of proteins were used for immunoprecipitation analysis. To pull down proteins interacting with CFTR, mAb596 antibodies cross-linked to Protein G agarose beads (Invitrogen) were incubated with cleared lysate for 1 h at 4°C. Beads were washed 3× with PBST lysis buffer. Bound proteins were eluted from beads via incubation with 2× SDS–PAGE sample buffer without reducing agent at 37°C for 15 min. Anti-FLAG M2 beads (Sigma-Aldrich, St. Louis, MO) were used to pull down proteins interacting with FLAG-tagged proteins. After washing, proteins bound were eluted with FLAG peptide. Eluted proteins were subjected to SDS–PAGE and Western blot analysis as described above.

CHX chase

To determine the steady-state level of different CFTR mutants, HEK293 cells were transfected and grown overnight prior to incubation with 5 µg/ml CHX (Sigma-Aldrich, St. Louis, MO) in the presence and absence of 15 µM CQ (Sigma-Aldrich, St. Louis, MO) or 10 µM bortezomib (LC Laboratories, Woburn, MA). Cells were harvested at indicated time points, and protein samples were prepared for Western blot analysis as described above.

Triton X-100 solubility assay

Harvested cell pellets were lysed in PBST (1% Triton X-100 in PBS) and separated into soluble and insoluble fractions by centrifugation at 20,000 × *g* for 30 min at 4°C. The insoluble fraction was resuspended in a 2× sample buffer with an equal volume of soluble fraction and sonicated. Total lysates, soluble fractions, and insoluble fractions were resolved with SDS–PAGE and subjected to Western blot analysis.

Disulfide cross-linking in whole cells

Cross-linking of Cys pairs introduced in Cys-less CFTR expressed in HEK293 cells was performed essentially as previously described (Serohijos *et al.*, 2008). Briefly, HEK cells transiently transfected with Cys-less CFTR constructs with Cys pairs introduced at CL/NBD interfaces were grown in 6-well plates. The cell was harvested in citric saline, and the cell pellet was washed in PBS and then resuspended in 30 µl PBS. Cell suspension (10 µl) was mixed with 20 µl PBS with DMSO as vehicle control or PBS containing 300 µM MTS cross-linker to yield a final concentration of 200 µM of bifunctional cross-linkers M3M (1,3-propanediyl bis-MTS) or M8M (1,5-pentanediyl bismethane-thiosulfonate) (Toronto Research Chemicals). After 15 min incubation at room temperature, the cross-linking reaction was stopped with 120 µl 1.5× Laemmli sample buffer without DTT. After sonication, 30 µl of the samples were loaded on 7.5% SDS–PAGE, and anti-CFTR mAb 596 was used for Western blotting.

Immunofluorescence microscopy

COS-7 cells were used for most of the microscopy study due to their flat and spread out nature, making them ideal for resolving intracellular organelles. COS-7 cells were grown on thin coverslips (Thermo Fisher Scientific 12541A) in 6-well plates. After transfection and treatment, cells were fixed at –20°C for 5 min with precooled methanol. Cells were rehydrated by washing 3× in PBS and blocked with 3% bovine serum albumin (BSA) in PBS for 30 min before immunostaining with various antibodies. Goat anti-mouse or goat anti-rabbit secondary antibodies with different fluorescent tags were used to detect proteins of interest. Coverslips were mounted onto slides using ProLong Diamond antifade mountant without (P36970) or with DAPI (P36971) (Invitrogen). Slides were allowed to dry in the dark at room temperature for at least 12 h before imaging with an IX81 motorized inverted microscope (Olympus, Center Valley, PA) equipped with standard DAPI (blue), FITC (green), TRITC (red), Cyan (far red) filter cubes. STED images were collected with a Leica TCS SP8 3× equipped and a FOV scanner. Acquired images were deconvoluted using CellSens Software (San Jose, CA) to remove background noise. Statistical analysis of signal colocalization was achieved through the calculation of Pearson's correlation coefficients. An ROI was manually drawn and cropped around the cell of interest, followed by extraction of the in-focus plane. The Coloc 2′ plugin for Fiji/ImageJ was then used to calculate Pearson's correlation coefficients between eGFP-CFTR and different sets of markers.

Live cell imaging

COS-7 cells were cultured in 35-mm glass-bottom dishes (MatTek P35G-1.5-10-C). After overnight transfection with fluorescent-tagged proteins, cells were rinsed with FluorBrite DMEM (Life Technologies Life Sciences) and kept in the same medium during drug treatment and imaging. Live-cell imaging was carried out using a ZEISS 880 microscope equipped with an AIRYSCAN detector that was outfitted with a humidified incubation chamber set to 37°C. Images were acquired and deconvoluted using CellSens software (Olympus) and processed with ICY and Adobe Photoshop.

Measurement of CFTR activity in Ussing chambers

Ion transport measurements with HBEs were performed in modified Ussing chambers (Physiologic Instruments) under voltage clamp conditions using Acquire & Analyze (version 2.3) software (Physiologic Instruments). Reference measurements (potential difference [P_d]) and transepithelial resistance (R_t) were obtained for each culture. Short circuit current (I_{sc}) was measured every 20 s and recorded digitally after bilateral equilibration at pH 7.4 for 10 min in 5 ml of pH 7.4 Krebs Bicarbonate Ringers (KBR; 115 NaCl mM, 25 $NaHCO_3$ mM, 2.4 K_2HPO_4 mM, 1.2 $CaCl_2$ mM, 1.2 $MgCl_2$ mM, 0.4 KH_2PO_4 mM, and 5 D-glucose mM). Chamber temperature was maintained at 36°C ± 1°C by a circulating water bath, and KBR was bubbled with 95% O_2-5% CO_2 throughout the experiment.

Agonists and inhibitors used to modulate CFTR activity were purchased from Sigma Chemical. In the presence of amiloride (100 µM, apical), forskolin (10 µM) was applied bilaterally to induce cAMP

activation of CFTR, and VX-770 (5 μM, apical) was applied to further activate CFTR. Currents detected were sensitive to the CFTR channel blocker $CFTR_{inh}$-172 (10 μM apical). As an internal control, UTP (100 μM) was used to activate calcium-activated chloride channels (CaCC) at the conclusion of the experiment. Data were exported and analyzed in Microsoft Excel, and slope values were subtracted for accuracy when necessary. Mean, SD, and SE measurements were calculated for each culture. Statistical analysis was by the Student's *t* test. $P < 0.05$ was considered to indicate statistical significance at 95% confidence and a $P < 0.001$ for 99% confidence. Line and bar graphs were created using Origin 8.6 software (OriginLab).

Membrane isolation and planar bilayer-based single-channel recording

BHK cells stabling expressing N1303K-CFTR with or without stabilizing mutations H1402S and ΔRI/2PT/H1402S were grown to 90% confluency, and cells were moved to a 27°C CO_2 incubator and grown with 3 μM VX-809 for 24 h. Cells were harvested and homogenized on ice in 10 mM HEPES, pH 7.2, and 1 mM EDTA containing a protease inhibitor cocktail. Centrifugation at 3000 × *g* for 5 min removed nuclei and undisrupted cells. The supernatant was centrifuged at 100,000 × *g* for 30 min to pellet membranes, which were then resuspended in phosphorylation buffer (10 mM HEPES, pH 7.2 containing 0.5 mM EGTA, 2 mM $MgCl_2$, and 250 mM sucrose).

Planar lipid bilayers were prepared by painting a 0.2-mm hole drilled in a Teflon cup with a phospholipid solution in n-decane containing a 3:1 mixture of 1-palmitoyl-2-oleoyl-sn-glycerol-3-phosphoethanolamine and 1-palmitoyl-2-oleoylsn-glycerol-3-phosphoserine (Avanti Polar Lipids). The lipid bilayer separated 1.0 ml of solution (cis side) from 5.0 ml of solution (trans side). Both chambers were magnetically stirred and thermally insulated. Heating and temperature were controlled with a Temperature Control System TC2BIP (Cell Micro Controls). CFTR ion channels were transferred into the preformed lipid bilayer by spontaneous fusion of membrane vesicles containing CFTR. To maintain uniform orientation and functional activity of CFTR channels, 2 mM ATP, 50 nM PKA, and membrane vesicles were added to the cis compartment only. All measurements were done in symmetrical salt solution (300 mM Tris/HCl; pH 7.2; 3 mM $MgCl_2$, and 1 mM EGTA) under voltage-clamp conditions using an Axopatch 200B amplifier (Axon Instrument/Molecular Device). The membrane voltage potential of –75 mV is the difference between cis and trans (ground) compartments. The output signal was filtered with an 8-pole Bessel low-pass filter LPBF-48DG (NPI Electronic, Tamm, Germany) with a cut-off frequency of 50 Hz, digitized with a sampling rate of 500 Hz, and recorded with pClamp9.2software. Origin 75 software (OriginLab, Northampton, MA) was used to fit all-points histograms (pClamp 9.2, Axon Instruments) by multi-peak Gaussians. Single-channel current was defined as the distance between peaks on the fitting curve and used for the calculation of the single-channel conductance. The probability of the single channel being open (P_o) was calculated as a ratio of the area under the peak for the open state to the total area under both peaks on the fitting curve.

ACKNOWLEDGMENTS

This work was supported by grants from the Cystic Fibrosis Foundation (CYR18XX0, BOUCHE19R0, GENTZS19I0) and NIH (GM056981 and P03DK065988). FRAP and STED Images were collected with the assistance of the UNC Hooker and Neuroscience Imaging Core facilities. Susan Boyle assisted with the culture of primary human bronchial epithelial cells.

REFERENCES

Axe EL, Walker SA, Manifava M, Chandra P, Roderick HL, Habermann A, Griffiths G, Ktistakis NT (2008). Autophagosome formation from membrane compartments enriched in phosphatidylinositol 3-phosphate and dynamically connected to the endoplasmic reticulum. J Cell Biol 182, 685–701.

Behnke J, Mann MJ, Scruggs FL, Feige MJ, Hendershot LM (2016). Members of the Hsp70 family recognize distinct types of sequences to execute ER quality control. Mol Cell 63, 739–752.

Buchberger A (2014). ERQC autophagy: Yet another way to die. Mol Cell 54, 3–4.

Clancy JP, Cotton CU, Donaldson SH, Solomon GM, VanDevanter DR, Boyle MP, Gentzsch M, Nick JA, Illek B, Wallenburg JC, *et al.* (2019). CFTR modulator theratyping: Current status, gaps, and future directions. J Cyst Fibros 18, 22–34.

Cutting GR (2017). Treating specific variants causing cystic fibrosis. J Am Med Assoc 318, 2130–2131.

Cyr DM (2005). Arrest of CFTRDeltaF508 folding. Nat Struct Mol Biol 12, 2–3.

Cyr DM, Hohfeld J, Patterson C (2002). Protein quality control: U-box-containing E3 ubiquitin ligases join the fold. Trends Biochem Sci 27, 368–375.

Dalal S, Rosser MF, Cyr DM, Hanson PI (2004). Distinct roles for the AAA ATPases NSF and p97 in the secretory pathway. Mol Biol Cell 15, 637–648.

Daniels R, Kurowski B, Johnson AE, Hebert DN (2003). N-linked glycans direct the co-translational folding pathway of influenza hemagglutinin. Mol Cell 11, 79–90.

Denning GM, Anderson MP, Amara JF, Marshall J, Smith AE, Welsh MJ (1992). Processing of mutant cystic fibrosis transmembrane conductance regulator is temperature-sensitive [see comments]. Nature 358, 761–764.

Donaldson SH, Pilewski JM, Griese M, Cooke J, Viswanathan L, Tullis E, Davies JC, Lekstrom-Himes JA, Wang LT, Group VXS (2018). Tezacaftor/Ivacaftor in subjects with cystic fibrosis and F508del/F508del-CFTR or F508del/G551D-CFTR. Am J Respir Crit Care Med 197, 214–224.

Doonan LM, Guerriero CJ, Preston GM, Buck TM, Khazanov N, Fisher EA, Senderowitz H, Brodsky JL (2019). Hsp104 facilitates the endoplasmic-reticulum-associated degradation of disease-associated and aggregation-prone substrates. Protein Sci 28, 1290–1306.

Forrester A, De Leonibus C, Grumati P, Fasana E, Piemontese M, Staiano L, Fregno I, Raimondi A, Marazza A, Bruno G, *et al.* (2019). A selective ER-phagy exerts procollagen quality control via a Calnexin-FAM134B complex. EMBO J 38.

Fregno I, Molinari M (2018). Endoplasmic reticulum turnover: ER-phagy and other flavors in selective and non-selective ER clearance. F1000Res 7, 454.

Fujita E, Kouroku Y, Isoai A, Kumagai H, Misutani A, Matsuda C, Hayashi YK, Momoi T (2007). Two endoplasmic reticulum-associated degradation (ERAD) systems for the novel variant of the mutant dysferlin: ubiquitin/proteasome ERAD(I) and autophagy/lysosome ERAD(II). Hum Mol Genet 16, 618–629.

Fulcher ML, Gabriel S, Burns KA, Yankaskas JR, Randell SH (2005). Well-differentiated human airway epithelial cell cultures. Methods Mol Med 107, 183–206.

Gautier C, Troilo F, Cordier F, Malagrino F, Toto A, Visconti L, Zhu Y, Brunori M, Wolff N, Gianni S (2020). Hidden kinetic traps in multidomain folding highlight the presence of a misfolded but functionally competent intermediate. Proc Natl Acad Sci USA 117, 19963–19969.

Gentzsch M, Ren HY, Houck SA, Quinney NL, Cholon DM, Sopha P, Chaudhry IG, Das J, Dokholyan NV, Randell SH, Cyr DM (2016). Restoration of R117H CFTR folding and function in human airway cells through combination treatment with VX-809 and VX-770. Am J Physiol Lung Cell Mol Physiol 311, L550–L559.

Grove DE, Fan CY, Ren HY, Cyr DM (2011). The endoplasmic reticulum-associated Hsp40 DNAJB12 and Hsc70 cooperate to facilitate RMA1 E3-dependent degradation of nascent CFTRDeltaF508. Mol Biol Cell 22, 301–314.

Grove DE, Rosser MF, Ren HY, Naren AP, Cyr DM (2009). Mechanisms for rescue of correctable folding defects in CFTRDelta F508. Mol Biol Cell 20, 4059–4069.

He L, Kota P, Aleksandrov AA, Cui L, Jensen T, Dokholyan NV, Riordan JR (2013). Correctors of DeltaF508 CFTR restore global conformational maturation without thermally stabilizing the mutant protein. FASEB J 27, 536–545.

Houck SA, Cyr DM (2012). Mechanisms for quality control of misfolded transmembrane proteins. Biochim Biophys Acta 1818, 1108–1114.
Houck SA, Ren HY, Madden VJ, Bonner JN, Conlin MP, Janovick JA, Conn PM, Cyr DM (2014). Quality control autophagy degrades soluble ERAD-resistant conformers of the misfolded membrane protein GnRHR. Mol Cell 54, 166–179.
Joo JH, Dorsey FC, Joshi A, Hennessy-Walters KM, Rose KL, McCastlain K, Zhang J, Iyengar R, Jung CH, Suen DF, *et al.* (2011). Hsp90-Cdc37 chaperone complex regulates Ulk1- and Atg13-mediated mitophagy. Mol Cell 43, 572–585.
Keating D, Marigowda G, Burr L, Daines C, Mall MA, McKone EF, Ramsey BW, Rowe SM, Sass LA, Tullis E, *et al.* (2018). VX-445-Tezacaftor-Ivacaftor in patients with cystic fibrosis and one or two Phe508del Alleles. N Engl J Med 379, 1612–1620.
Kirk KL, Wang W (2011). A unified view of cystic fibrosis transmembrane conductance regulator (CFTR) gating: combining the allosterism of a ligand-gated channel with the enzymatic activity of an ATP-binding cassette (ABC) transporter. J Biol Chem 286, 12813–12819.
Klaips CL, Jayaraj GG, Hartl FU (2018). Pathways of cellular proteostasis in aging and disease. J Cell Biol 217, 51–63.
Kruse KB, Brodsky JL, McCracken AA (2006). Autophagy: an ER protein quality control process. Autophagy 2, 135–137.
Ktistakis NT (2020). ER platforms mediating autophagosome generation. Biochim Biophys Acta Mol Cell Biol Lipids 1865.
Li K, Jiang Q, Bai X, Yang YF, Ruan MY, Cai SQ (2017). Tetrameric assembly of K(+) channels requires ER-located chaperone proteins. Mol Cell 65, 52–65.
Matsunaga K, Morita E, Saitoh T, Akira S, Ktistakis NT, Izumi T, Noda T, Yoshimori T (2010). Autophagy requires endoplasmic reticulum targeting of the PI3-kinase complex via Atg14L. J Cell Biol 190, 511–521.
Meacham GC, Lu Z, King S, Sorscher E, Tousson A, Cyr DM (1999). The Hdj-2/Hsc70 chaperone pair facilitates early steps in CFTR biogenesis. EMBO J 18, 1492–1505.
Meacham GC, Patterson C, Zhang W, Younger JM, Cyr DM (2001). The Hsc70 co-chaperone CHIP targets immature CFTR for proteasomal degradation. Nat Cell Biol 3, 100–105.
Middleton PG, Mall MA, Drevinek P, Lands LC, McKone EF, Polineni D, Ramsey BW, Taylor-Cousar JL, Tullis E, Vermeulen F, *et al.* (2019). Elexacaftor-Tezacaftor-Ivacaftor for cystic fibrosis with a single Phe508del allele. N Engl J Med 381, 1809–1819.
Omari S, Makareeva E, Roberts-Pilgrim A, Mirigian L, Jarnik M, Ott C, Lippincott-Schwartz J, Leikin S (2018). Noncanonical autophagy at ER exit sites regulates procollagen turnover. Proc Natl Acad Sci USA 115, E10099–E10108.
Oren YS, Pranke IM, Kerem B, Sermet-Gaudelus I (2017). The suppression of premature termination codons and the repair of splicing mutations in CFTR. Curr Opin Pharmacol 34, 125–131.
Pickles S, Vigie P, Youle RJ (2018). Mitophagy and quality control mechanisms in mitochondrial maintenance. Curr Biol 28, R170–R185.
Pohl C, Dikic I (2019). Cellular quality control by the ubiquitin-proteasome system and autophagy. Science 366, 818–822.
Qian SB, McDonough H, Boellmann F, Cyr DM, Patterson C (2006). CHIP-mediated stress recovery by sequential ubiquitination of substrates and Hsp70. Nature 440, 551–555.
Ren HY, Grove DE, De La Rosa O, Houck SA, Sopha P, Van Goor F, Hoffman BJ, Cyr DM (2013). VX-809 corrects folding defects in cystic fibrosis transmembrane conductance regulator protein through action on membrane-spanning domain 1. Mol Biol Cell 24, 3016–3024.
Rosser MF, Grove DE, Chen L, Cyr DM (2008). Assembly and misassembly of cystic fibrosis transmembrane conductance regulator: folding defects caused by deletion of F508 occur before and after the calnexin-dependent association of membrane spanning domain (MSD) 1 and MSD2. Mol Biol Cell 19, 4570–4579.
Serohijos AW, Hegedus T, Aleksandrov AA, He L, Cui L, Dokholyan NV, Riordan JR (2008). Phenylalanine-508 mediates a cytoplasmic-membrane domain contact in the CFTR 3D structure crucial to assembly and channel function. Proc Natl Acad Sci USA 105, 3256–3261.
Singh AK, Fan Y, Balut C, Alani S, Manelli AM, Swensen AM, Jia Y, Neelands TR, Vortherms TA, Liu B, *et al.* (2020). Biological characterization of F508delCFTR protein processing by the CFTR corrector ABBV-2222/GLPG2222. J Pharmacol Exp Ther 372, 107–118.
Sopha P, Ren HY, Grove DE, Cyr DM (2017). Endoplasmic reticulum stress-induced degradation of DNAJB12 stimulates BOK accumulation and primes cancer cells for apoptosis. J Biol Chem 292, 11792–11803.
Tooze SA, Yoshimori T (2010). The origin of the autophagosomal membrane. Nat Cell Biol 12, 831–835.
Van Goor F, Yu H, Burton B, Hoffman BJ (2014). Effect of ivacaftor on CFTR forms with missense mutations associated with defects in protein processing or function. J Cyst Fibros 13, 29–36.
Vargas JNS, Wang C, Bunker E, Hao L, Maric D, Schiavo G, Randow F, Youle RJ. (2019). Spatiotemporal Control of ULK1 activation by NDP52 and TBK1 during selective autophagy. Mol Cell 74, 347–362 e346.
Veit G, Avramescu RG, Chiang AN, Houck SA, Cai Z, Peters KW, Hong JS, Pollard HB, Guggino WB, Balch WE, *et al.* (2016). From CFTR biology toward combinatorial pharmacotherapy: expanded classification of cystic fibrosis mutations. Mol Biol Cell 27, 424–433.
Veit G, Roldan A, Hancock MA, Da Fonte DF, Xu H, Hussein M, Frenkiel S, Matouk E, Velkov T, Lukacs GL (2020). Allosteric folding correction of F508del and rare CFTR mutants by elexacaftor-tezacaftor-ivacaftor (Trikafta) combination. JCI Insight 5.
Wilkinson S (2019). Emerging principles of selective ER autophagy. J Mol Biol.
Yla-Anttila P, Vihinen H, Jokitalo E, Eskelinen EL (2009). 3D tomography reveals connections between the phagophore and endoplasmic reticulum. Autophagy 5, 1180–1185.
Younger JM, Chen L, Ren HY, Rosser MF, Turnbull EL, Fan CY, Patterson C, Cyr DM (2006). Sequential quality-control checkpoints triage misfolded cystic fibrosis transmembrane conductance regulator. Cell 126, 571–582.
Yu H, Burton B, Huang CJ, Worley J, Cao D, Johnson JP Jr., Urrutia A, Joubran J, Seepersaud S, Sussky K, *et al.* (2012). Ivacaftor potentiation of multiple CFTR channels with gating mutations. J Cyst Fibros 11, 237–245.
Zachari M, Gudmundsson SR, Li Z, Manifava M, Shah R, Smith M, Stronge J, Karanasios E, Piunti C, Kishi-Itakura C, *et al.* (2019). Selective autophagy of mitochondria on a ubiquitin-endoplasmic-reticulum platform. Dev Cell 50, 627–643.
Zhang F, Kartner N, Lukacs GL (1998). Limited proteolysis as a probe for arrested conformational maturation of delta F508 CFTR. Nat Struct Biol 5, 180–183.